The Geology and Petrology of the Rognsund Intrusion, West Finnmark, Northern Norway

B. ROBINS

Robins, B. 1982: The geology and petrology of the Rognsund intrusion, West Finnmark, northern Norway. *Norges geol. Unders. 371*, 1–55.

The Rognsund intrusion is an early-Caledonian gabbroic body containing an 800 m-thick sequence of metamorphosed cumulates. Well-developed rhythmic layering is interpreted in terms of both *in situ* crystallization and deposition from crystal suspensions. Relict cumulus plagioclase shows a variation from An_{85} to An_{65} through the cumulate sequence, clinopyroxene exhibits iron-enrichment from Ca_{47} Mg_{44} Fe_9 to Ca_{49} Mg_{35} Fe_{16} and olivine varies from Fo_{74} to Fo_{65}. The diopside/salite exhibits a highly systematic chemical trend and contains as much as 7.0% Al_2O_3 and 1.2% TiO_2. It never co-existed with a primary Ca-poor pyroxene. Cumulus Fe–Ti oxides appeared at an early fractionation stage.

Average cumulates and a marginal chill are all ne-normative. FeO decreases upwards in the cumulates until the abrupt appearance of oxides increases FeO, Fe_2O_3 and TiO_2, while FeO/MgO increases upwards. FeO in normative di and ol falls systematically through the cumulate sequence. The alkali-enrichment fractionation trend is attributed to the crystallization of olivine and clinopyroxene. The chill is not considered to be representative of the parental magma. The mineralogy and fractionation trend of the intrusion is, however, consistent with a critically undersaturated basalt parent which may be petrogenetically related to the alkaline olivine basalt to picrite dykes emplaced into the gabbro after its deformation.

B. Robins, Geologisk Institutt, avd. A, Realfagbygget, 5014 Universitetet i Bergen, Norway

Introduction

Of the many layered mafic intrusions described in petrological literature, few are generally accepted as illustrating the solid fractionation products of an alkali olivine basalt parent. An account dealing with the Blue Mountain complex (Grapes 1975) provides a detailed analysis of the natural low-pressure crystallization of such a magma, and alkali basalts have been inferred to be parental to the layered rocks of the Canary Islands (Gastesi 1969, Cendrero 1970), though this has been questioned by Brown (in discussion of Gastesi 1969), the Lilloise intrusion of east Greenland (Brown 1973), and the syn-orogenic 'clinopyroxene gabbros' of Northern Norway (Robins & Gardner 1974, Robins 1975). This account deals with a small, conveniently exposed part of the Rognsund intrusion (Fig. 1 & Plate 1), one of the clinopyroxene gabbro layered complexes. Earlier studies of this and similar bodies within the Seiland province (Barth 1953, Krauskopf 1954, Oosterom 1963) concluded that they had their origin in the granulite-facies metamorphism, or anatexis, of volcanic sequences.

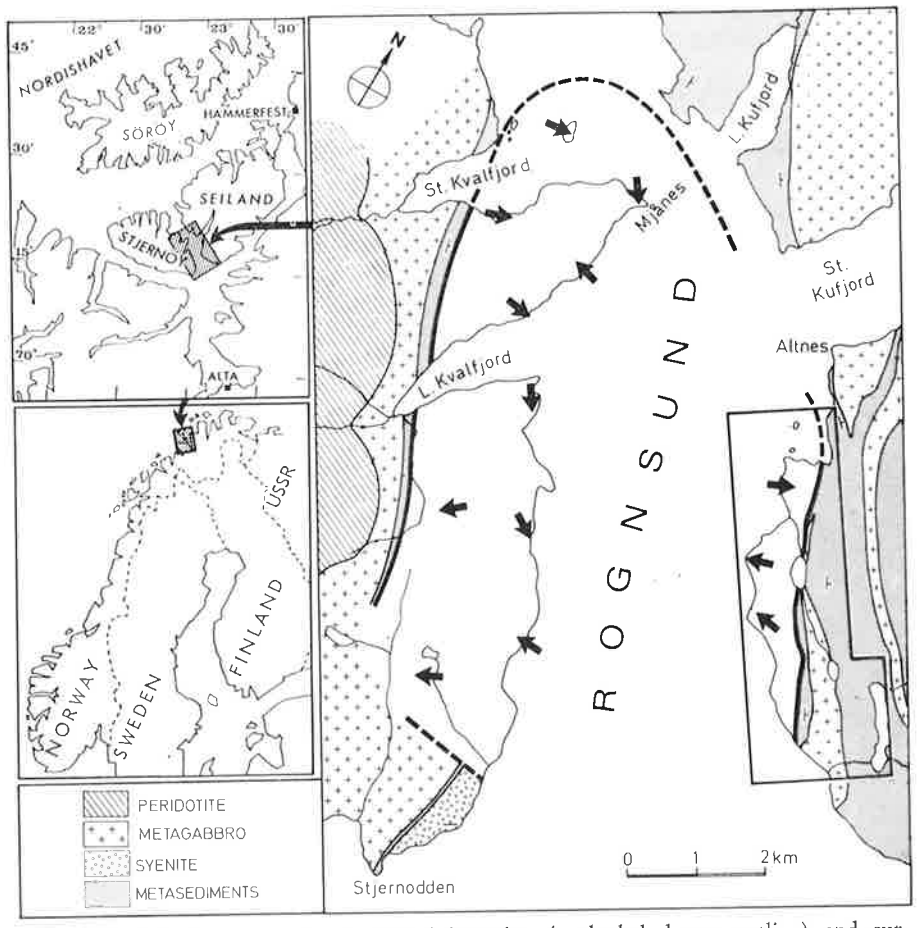

Fig. 1. Simplified map of the Rognsund intrusion (unshaded, heavy outline) and surroundings. Thick arrows give the direction of dip of the steep rhythmic layering. Area of Plate 1 is outlined.

General geology

The Rognsund intrusion is exposed along the southwestern coastline of the island of Seiland and the opposing coast of Stjernøy in the West Finnmark district of northern Norway (Fig. 1). It was emplaced during the second major phase of Caledonian deformation into gneissic quartzo–feldspathic metasediments undergoing Barrovian almandine–amphibolite facies metamorphism. It occupies a rough oval, 50 km² in area, the majority of which is hidden beneath fjords; the synformal structure of the intrusion, and the irregular, usually steep, orientation of internal structures, was probably the result of gravitational deformation which took place later than crystallization of the intrusion. In the Hakkstabben area (Plate 1) the Rognsund intrusion was pre-dated by a concordant metagabbro of tholeiitic aspect which was emplaced during the course of the first phase of deformation, by a small mesoperthite syenite (perthosite) possibly related to layered syenogabbro complexes cropping out elsewhere in

the Seiland Province (Robins & Gardner 1974), and by mafic dykes. During later tectonic events, a metamorphic fabric was imposed on parts of the intrusion, and the internal layering was rotated to steep orientations. Mafic dykes belonging to an alkali olivine basalt suite (Robins 1975, Robins & Takla 1979), alkaline pyroxenite dykes (Robins 1974), and amphibole- or biotite-bearing syenite and nepheline syenite pegmatites (Barth 1927, Robins 1972) all cross-cut the intrusion. These later dykes are themselves variably deformed and show petrographic evidence of continuing metamorphism in the amphibolite facies. Alkaline rocks are accompanied by narrow metasomatic aureoles in which the host is converted either to ultramafic or silicocarbonatitic fenites (Robins & Tysseland 1979).

Rb–Sr isochrons obtained on the adjacent island of Sørøy from mobilisates in the contact metamorphic aureoles of mafic intrusions emplaced early in the Caledonian orogenic evolution, and from regionally-developed, alkaline minor intrusives suggest that emplacement of the Rognsund intrusion took place between 523 ± 21 m.y. and 490 ± 27 m.y. ago (Sturt et al. 1978, recalculated to $\lambda\,^{87}\mathrm{Rb} = 1.42 \times 10^{-11}\ \mathrm{y}^{-1}$).

Contact metamorphism

The contact-metamorphic aureole developed in metasediments in contact with the Rognsund intrusion is over 250 m wide and may be divided into two zones: An outer, hornfelsic zone; and an inner zone, up to 160 m across, in which rheomorphic breccias are developed (Plate 1). The unusually thorough anatexis was a result of the persistence of high temperatures, and the shallow thermal gradients consequent on the superimposition of contact metamorphism on regional metamorphism in the almandine–sillimanite–orthoclase subfacies. The thermal models of Jaeger (1957, 1964) and Irvine (1970) show clearly that the metamorphic temperatures attained in the inner part of a contact aureole are higher and longer-lasting when magma is emplaced into a hot environment than into cooler host rocks.

In the outer, hornfelsic, part of the Rognsund aureole, the regional-metamorphic assemblage of quartz, alkali feldspar, plagioclase, garnet, biotite and sillimanite is replaced by an equivalent, dehydrated paragenesis containing orthopyroxene, hercynitic spinel and rutile in place of biotite. In thin pelitic and semipelitic horizons these minerals may be accompanied by corundum and also cordierite, which clearly co-existed with garnet. Pre-hornfelsing structures, such as D_1 and early-D_2 folds, are preserved and date the contact metamorphism relative to the tectono-thermal development established outside the aureole. Mafic dykes, which before emplacement of the Rognsund intrusion had been partially or totally amphibolitized, developed pyroxene–granulite rinds following both primary and tectonic contacts (see Robins & Takla 1979). In zones a few centimetres wide along the margins of these dykes the hornfelses may be coarser grained than elsewhere and retain biotite as a stable phase. It is believed that the slow dehydration of the mafic rocks was due to the

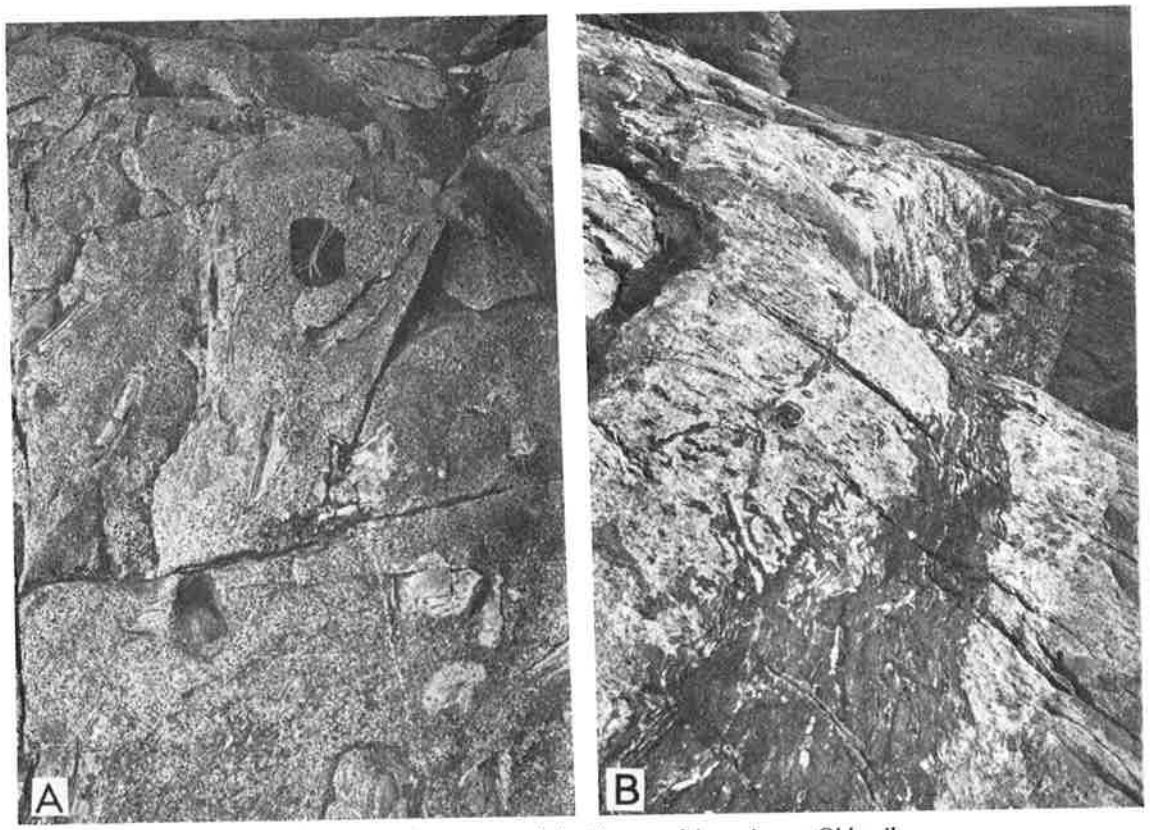

Fig. 2. (A) Granitoid anatexite close to the contact of the Rognsund intrusion at Oldervik, with enclosed restites of calc-silicate, quartzite and disrupted pre-anatexis mafic dykes. (B) Schistose amphibolite, feldspathized and intruded by pegmatoid neosome during anatexis of the surrounding psammitic metasediments in the inner part of the contact metamorphic aureole. Note that the anatexites contain large amphiboles only in the vicinity of such pre-anatexis dykes. Light meter used for scale measures 9 x 6 cm.

sluggishness of the outward diffusion of H_2O. Diffusion could maintain a sufficiently high P_{H2O} in the immediately adjacent hornfelses for biotite to remain stable and for enhanced grain growth. Elsewhere the hornfelses were dehydrated due to the presence of anatectic melts, whose existence is suggested by coarse-grained garnet- and biotite-bearing granitic material present as irregular segregations within the hornfelses and as back-veins in the mafic dykes.

Within the inner zone of the aureole almost all traces of original lithological banding are progressively lost; horizons of suitable composition have undergone thorough mobilization. Pre-mobilization mafic dykes roughly concordant with the contact of the Rognsund intrusion underwent boudinage where originally little foliated, or were invaded by neosome along the tectonic fabric and partly disrupted where originally schistose (Fig. 2 B). Some cross-cutting dykes were folded and back-veins of the neosome were injected parallel to the axial planes. The mobilizates are represented by a rather massive garnet-, orthopyroxene- and more rarely cordierite-bearing granitoid neosome containing enclaves of extreme composition (Fig. 2 A), usually quartzite and calc-silicates, but also including feldspar-rich rocks, fragments of disrupted mafic dykes and Al-rich xenoliths. The Al-rich xenoliths have the most complex parageneses, containing plagioclase feldspar, garnet, sillimanite, cordierite, hercynite (almost invariably enclosed in sillimanite), and occasionally corundum. Apart from the mafic dyke xenoliths, the enclaves are interpreted as restites derived from the anatexis of metasediments.

Eleven analyses of the neosome developed in the inner aureole (Table 1)

Table 1. Major- and trace-element analyses of metapsammites and contact anatexites

	1	2	3	4	5	6	7	8	9	10	11	12	13	14
SiO_2	63.40	63.47	63.26	59.19	61.27	62.23	62.54	64.29	64.78	66.11	68.54	69.14	72.43	72.59
TiO_2	1.07	1.09	1.20	1.36	1.23	1.26	1.28	1.43	1.16	1.02	1.01	1.11	0.89	0.93
Al_2O_3	16.58	15.76	17.46	18.64	18.63	15.38	17.97	14.00	25.68	15.48	14.07	13.99	13.82	11.23
Fe_2O_3	3.14	3.16	6.16	3.96	2.82	1.36	5.99	5.25	6.37	6.03	1.97	4.99	2.95	4.28
FeO	5.60	4.81	1.66	4.34	4.70	6.33	1.52	2.86	1.27	0.98	3.40	1.27	0.72	1.48
MnO	0.16	0.16	0.12	0.12	0.12	0.15	0.11	0.16	0.13	0.12	0.10	0.08	0.07	0.11
MgO	2.26	2.36	2.01	2.36	2.29	2.69	1.99	2.53	1.84	1.86	1.74	1.61	1.06	1.48
CaO	1.86	1.99	2.16	2.49	2.09	2.75	1.77	3.63	2.06	1.88	2.01	1.30	1.63	2.21
Na_2O	2.50	2.40	2.35	3.40	3.25	3.40	3.00	3.80	2.80	2.98	2.93	2.40	2.30	2.63
K_2O	3.27	2.80	2.99	3.63	4.14	3.41	4.53	0.76	3.07	3.67	3.50	3.57	4.05	2.59
P_2O_5	0.21	0.12	0.22	0.08	0.07	0.08	0.11	0.03	0.09	0.08	0.10	0.05	0.05	0.05
H_2O+	0.50	0.40	0.65	0.40	0.38	0.89	0.20	0.48	0.53	0.25	0.76	0.40	0.30	0.36
TOTAL	100.55	98.52	100.24	99.97	100.99	99.93	101.01	99.22	99.78	100.46	100.13	99.81	100.27	99.94
FeO+	8.43	7.65	7.20	7.90	7.24	7.55	6.91	7.59	7.00	6.41	5.17	5.76	3.38	5.33
ppm														
Rb	124	111	82	79	90	62	111	10	76	71	74	69	108	53
Sr	226	237	226	335	273	517	291	407	293	329	268	269	306	369
Y	47	43	50	43	51	36	51	25	46	45	38	50	44	19
Zr	338	349	392	441	389	396	425	571	419	338	396	722	578	356
Nb	24	21	25	33	23	29	25	43	23	19	20	23	20	17
La	53	51	61	70	47	52	65	34	43	41	38	45	40	41
Ce	95	93	109	107	80	91	113	57	82	78	82	76	72	74
Nd	54	49	62	60	43	45	64	26	43	41	42	46	40	39
C.I.P.W. norms														
Q	26.8	29.2	31.2	15.7	16.8	15.8	21.3	27.8	29.8	28.8	30.0	36.5	38.6	40.6
or	19.3	16.6	17.7	21.5	24.5	20.2	26.8	4.5	18.1	21.7	20.7	21.1	23.9	15.3
ab	21.2	20.3	19.9	28.8	27.5	28.8	25.4	32.2	23.7	25.2	24.8	20.3	19.5	22.3
an	7.8	9.1	9.3	11.8	9.9	13.1	8.1	17.8	9.6	8.8	0.3	6.1	7.8	10.6
C	6.0	5.5	7.0	4.8	5.2	1.3	5.2	0.4	4.2	3.4	2.0	3.9	2.8	0.2
en	5.6	5.9	5.0	5.9	5.7	6.7	5.0	6.3	4.6	4.6	4.3	4.0	2.6	3.7
fs	6.2	4.7	–	2.7	4.5	8.7	–	–	–	–	3.1	–	–	–
mt	4.6	4.6	2.3	5.7	4.1	2.0	1.6	5.6	1.2	0.6	2.9	1.4	–	2.4
hm	–	–	4.6	–	–	–	4.9	1.4	5.6	5.6	–	4.2	2.9	2.6
il	2.0	2.1	2.3	2.6	2.3	2.4	2.4	2.7	2.2	1.9	1.9	2.1	1.7	1.8
ap	0.5	0.3	0.5	0.2	0.2	0.2	0.3	0.1	0.2	0.2	0.2	0.1	0.1	0.1
Q+or+ab	67.2	66.1	68.7	65.9	68.7	64.7	73.5	64.5	71.7	75.1	75.5	77.9	82.0	78.1
ab/an	2.7	2.2	2.1	2.4	2.8	2.2	3.2	1.8	2.5	2.9	2.7	3.3	2.5	2.1

1 & 2 Regionally-metamorphosed psammitic metasediments from the Hakkstabben area.
3. Contact-metamorphosed psammite from the outer zone of the Rognsund aureole.
4–14 Anatexites from the inner part of the Rognsund aureole.

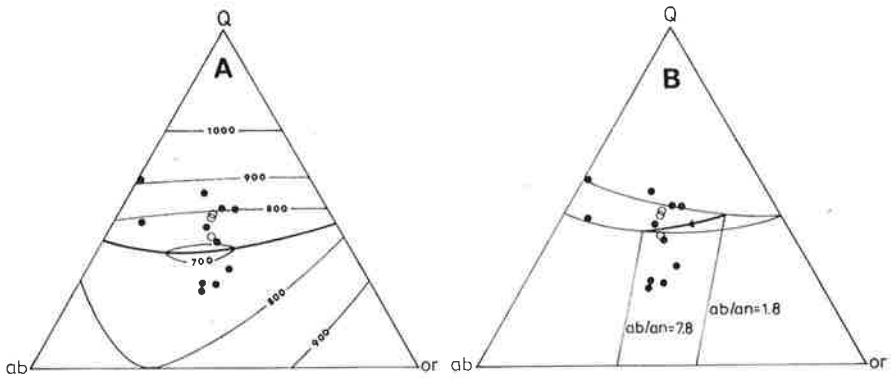

Fig. 3. Normative mineralogy of metasediments (open circles) and anatexites (filled circles) from the Hakkstabben aureole projected into the ternary and quaternary oversaturated residua systems (Tuttle & Bowen 1958, von Platen 1965). Cotectic lines and surfaces are for $P_{H2O} = 2$ kb.

display a variable chemistry in the granite–adamellite–granodiorite range. Some have compositions similar to those of analysed metapsammites affected only by regional metamorphism or hornfelsing, apparently indicating a high degree of equilibrium partial melting in certain lithologies. The neosomes, usually characterized by euhedral, zoned plagioclases poikilitically enclosed in alkali feldspar and quartz are, however, seldom free from small restite xenoliths, and garnet xenocrysts including fabrics and minerals different from the enclosing anatexites are ubiquitous. The appearance of C in the C.I.P.W. norms of the neosomes is mainly the result of the garnet xenocrysts and their hercynite or corundum inclusions.

Plotted in the ternary system quartz–albite–orthoclase, the neosomes do not group near water-saturated cotectic minima for confining pressures between 500 and 3000 bars. At $P_{H2O} = 2$ kb the majority are located within the isotherm for 900°C which must be a realistic minimum for the temperatures developed in the inner part of the metamorphic aureole. The neosome compositions are situated within the anorthite volume and close to cotectic surfaces in the quaternary system quartz–albite–orthoclase–anorthite (Fig. 3). The three-phase cotectic line in the system appears in projection to pass through the compositional field occupied by the metapsammites. The metapsammites also lie, however, within the plagioclase volume. The greater dispersion of the neosomes relative to the psammites suggests that fractional melting played a more important role in their genesis than equilibrium partial melting.

Layering

The Hakkstabben segment of the Rognsund intrusion exposes a cumulate sequence, nominally 800 m thick, in which rhythmic and cryptic layering are important components. Mineral and whole-rock compositions suggest that the succession represents only part of a much thicker cumulate sequence.

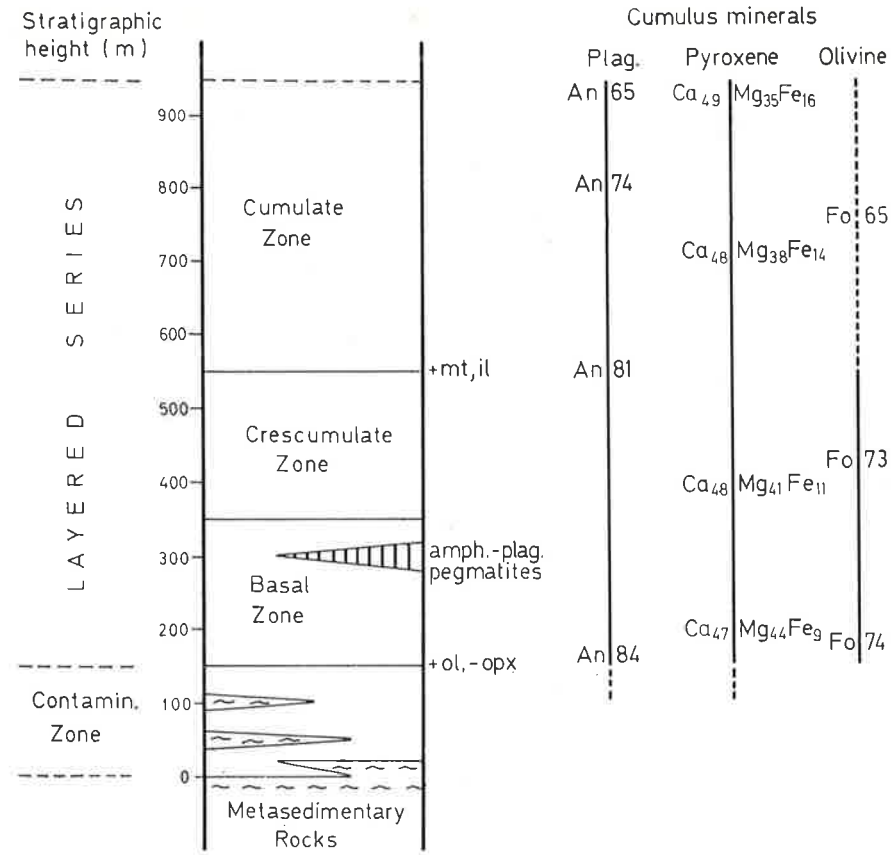

Fig. 4. Stratigraphic subdivisions of the Hakkstabben segment of the Rognsund intrusion, and generalized compositional variations in the main cumulus phases.

CRYPTIC LAYERING

The intrusion has been subdivided on the basis of major phase contacts and textural properties into four successive zones (Fig. 4).

The contaminated zone, in contact with rocks of the aureole with the intervention of a thin fine-grained chill, is occupied by banded and rather strongly metamorphosed olivine-free gabbros containing abundant xenoliths. The latter are usually lenticles a few centimetres in length and consist mainly of granular basic plagioclase showing strong reversed zonation. Hercynitic spinel and corundum are concentrated in the centres of the xenoliths. They are concentrated close to the contact with the aureole and appear to be restites derived from pelitic metasediments (Fig. 5). The xenoliths were probably of local derivation and incorporated during the initial stages of emplacement of the Rognsund magma. The general orientation of the xenoliths is parallel to the external contact of the intrusion, the streaky banding and the rhythmic layering present higher in the contaminated zone. This may be explained either by the flowage of the magma during intrusion, or by later settling of the xenoliths. Similar

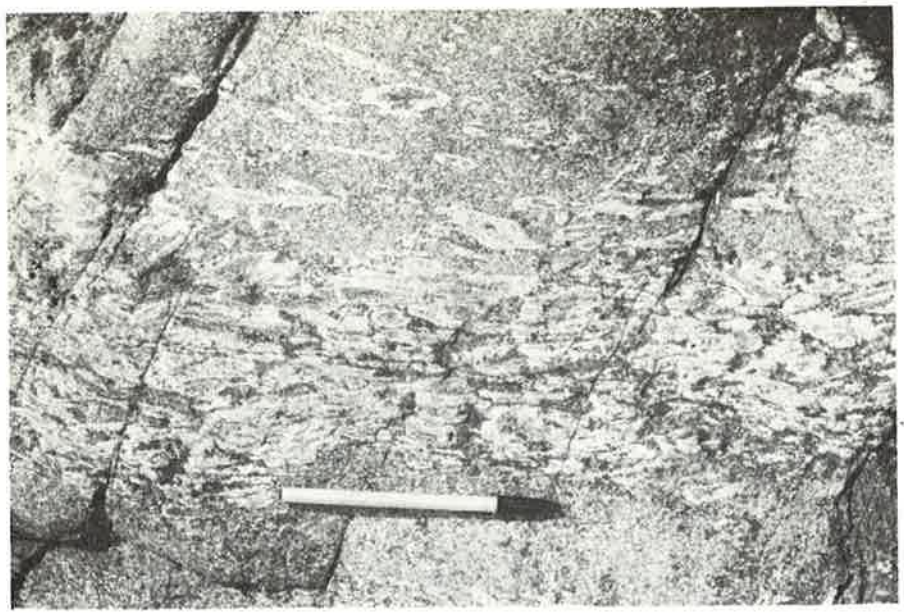

Fig. 5. Incompletely disrupted xenolith of pelitic derivation contained in gabbros of the contaminated zone, close to the base of the Rognsund intrusion. The lenticular areas are composed of basic plagioclase, hercynitic spinel and corundum, and in the large xenolith are surrounded by garnet and biotite.

xenoliths are present in both the marginal border group and the layered series of the nearby Lille Kufjord gabbro, where they appear to have settled (Robins & Gardner 1974, see especially Fig. 12).

The frequence of refractory xenoliths, the absence of olivine, the occurrence of quite abundant orthopyroxene in the hypersthene/bronzite range and some aspects of the major-element compositions may suggest that some of the gabbros in the outer part of the contaminated zone crystallized from a syntetic magma which had assimilated significant amounts of metasedimentary material. Towards the top of the zone, however, rhythmic layering is sporadically developed and macroscopic cumulate textures are preserved, plagioclase and clinopyroxene being the cumulus phases. There is some evidence that cumulus plagioclase becomes on average more Ca-rich upwards through the contaminated zone, although almost all samples also contain a metamorphic generation of more sodic plagioclase.

The thickness of the contaminated zone decreases northwards from a maximum of just over 200 m at Oldervik, and the zone is completely lacking over a distance of 500 m north of Skarvvand where the basal zone is in contact with a litchfieldite gneiss. The zone re-appears where the gneiss wedges out, and at Skarvnesstrand attains a thickness of 60 m. These variations may in part be of primary origin, but the disappearance of the contaminated zone north of Skarvvand is almost certainly due to shear along the originally pegmatitic litchfieldite.

The contaminated zone-basal zone contact is marked by the rather abrupt appearance of cumulus olivine.

The basal zone is occupied by olivine- and clinopyroxene-rich eucrites and picrites with poorly to moderately developed small-scale rhythmic layering. Small xenoliths of metasedimentary derivation are rare, although in the southern part of its outcrop the zone contains two large rafts of mobilized gneissic psammite (Plate 1). The upper part of the basal zone contains a discontinuous horizon along which comb-structured amphibole–plagioclase pegmatites are developed, described in more detail below. Crescumulate textures are absent from the basal zone.

The crescumulate zone contains olivine eucrites with strong rhythmic layering. The basal zone–crescumulate zone boundary is not marked by a phase contact; it has been mapped at the base of the first crescumulate layer. In both the crescumulate and the basal zone, plagioclases are highly calcic, while olivine compositions correspond to iron-rich chrysolite. Optical determinations of cumulus plagioclase compositions suggest a slight trend towards more sodic plagioclases upwards, while microprobe analyses of olivine show an almost constant composition. Clinopyroxene shows slight iron-enrichment through the two zones.

The cumulate zone is characterized by cumulus magnetite and ilmenite. Plagioclase is the principal cumulus phase; olivine and clinopyroxene are less important than in the underlying crescumulate and basal zones. Due to its originally limited mode and later instability, olivine is rarely observed in the rocks of the cumulate zone; in the main it is proxied by orthopyroxene–magnetite/ilmenite and pyroxene–hercynite symplectites. The clinopyroxenes of the cumulate zone are substantially depleted in TiO_2 and Al_2O_3 compared with those of the underlying zones, but upward iron-enrichment persists. Crescumulate olivine and pyroxene are absent from the cumulate zone. Plagioclase becomes more sodic through the cumulate zone and at the same time increases in abundance in average cumulates, the uppermost cumulates, exposed between Grandnes and Hakkstabholm (Plate 1), being anorthositic gabbros. The maximum observed thickness of the cumulate zone is approximately 400 m, the same as for the basal and crescumulate zones together.

RHYTHMIC LAYERING

Apart from the contaminated zone and certain parts of the basal zone, the bulk of the Rognsund gabbro in the Hakkstabben area contains layers of widely different character and mineralogical composition. Layers may be up to a few metres thick, but are usually less than 1 m, and are separated by ratio, phase or form contacts. Erosional and depositional structures other than layers and layer contacts, as well as post-depositional structures are sporadically developed. Due to coarse grain sizes, cumulus and intercumulus phases and their textural relationships can often be better determined at outcrop than in thin-section, where metamorphic textural re-organization usually dominates. In the following descriptions the identification of the cumulus phases is, therefore, mainly based

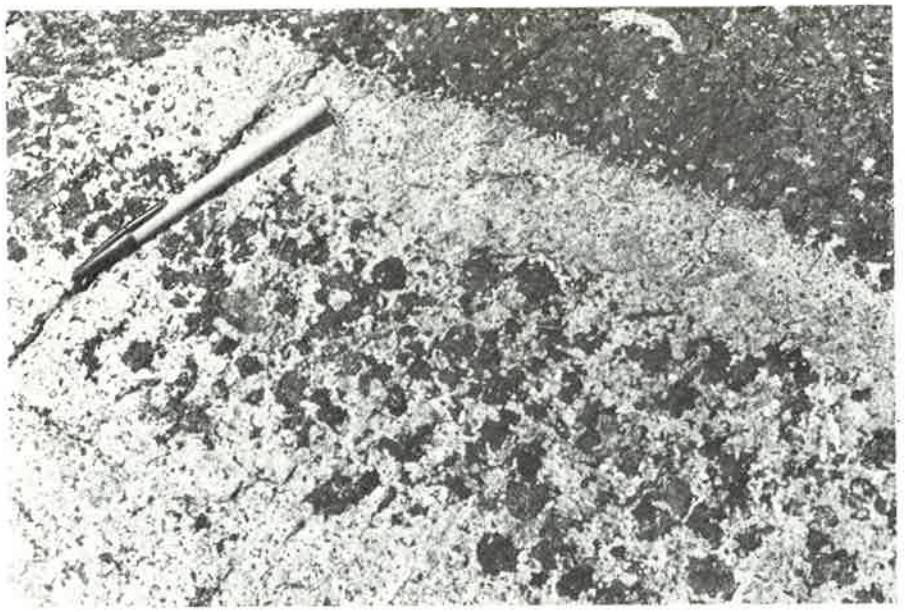

Fig. 6. Mineral-graded layer in which plagioclases are size-graded. Note the in-layer phase contact marking the exit of cumulus clinopyroxene, and the discrepancy in the sizes of pyroxenes and plagioclases, suggesting hydraulic disequilibrium. 'Up' in the cumulate sequence is towards the top of the photograph.

on macroscopic observations. Nomenclature follows the proposals of Jackson (1967).

Mineral- and size-graded layers are particularly well developed in the cumulate zone and in the upper part of the crescumulate zone. In individual layers, mineral- and size-grading are independent phenomena: A right way up mineral-graded layer may show reversed size-grading and vice versa. In consequence, neither are reliable indicators of 'way-up' in the cumulate sequence. Boundaries between graded layers are most usually either ratio or phase contacts; form contacts separate size-graded layers involving the same cumulus phases. Irregular phase contacts are also present in certain layers graded with respect to other minerals. Fig. 6 illustrates a phase contact marking the disappearance of cumulus clinopyroxene and olivine within a layer in which cumulus plagioclase is continuously size-graded. Extreme mineral-grading may also be accompanied by similar phase contacts, usually ones marking the exit of clinopyroxene and olivine such that the uppermost cumulates in certain layers are plagioclase heteradcumulates (Fig. 7). Goode (1976) attributes such 'paired' sets to differential settling of phases generated by discontinuous bursts of crystallization.

In many layers, large discrepancies in the sizes of olivine, clinopyroxene and plagioclase crystals suggest that the cumulus assemblages do not represent hydraulic equilibrium. In particular, cumulus clinopyroxenes are often many times larger in diameter than the accompanying plagioclases (Fig. 6), and certain isomodal layers contain clinopyroxenes of widely varying size. This feature may indicate that individual primocrysts were derived from separate regions in the magma chamber (Brown & Farmer 1972) or during different episodes of crystallization (Goode 1976).

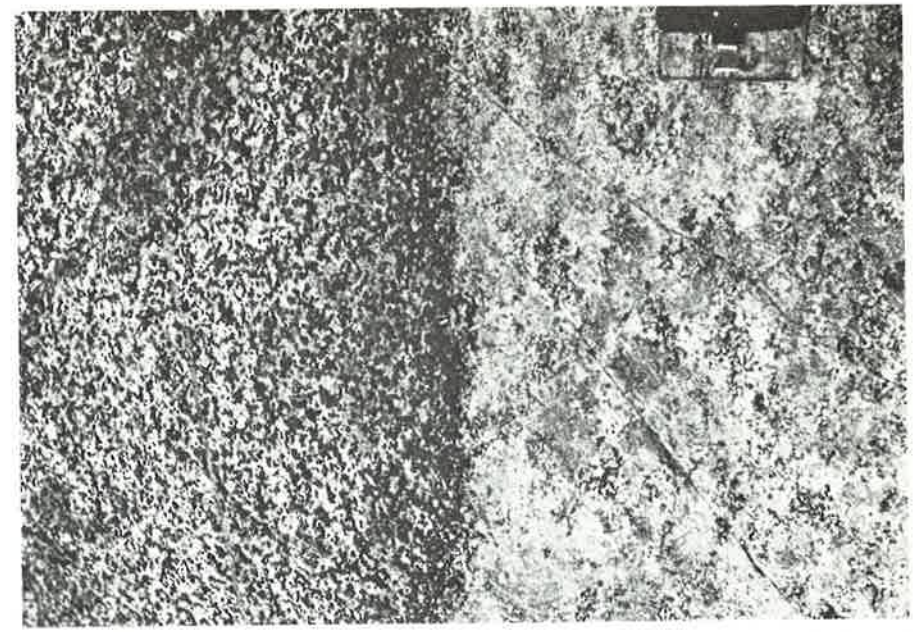

Fig. 7. Parts of two mineral-graded layers containing exit phase boundaries for olivine and clinopyroxene. Mineral-grading is exhibited by the lower parts of the layers (left-hand side of figure) while the upper parts are plagioclase cumulates with poikilitic clinopyroxene (right-hand side of figure). Edge of compass measures 6.5 cm.

Cumulates in the cumulate zone preserve a lamination of tablet-shaped plagioclase and clinopyroxene whereas this is rarely observed in the crescumulate zone. In the latter, plagioclase often forms equant crystals (Fig. 6). The reasons for this variation are unknown.

As noted earlier, the cumulate zone exhibits large-scale mineral-grading; the proportion of cumulus plagioclase increases with respect to clinopyroxene upwards in the stratigraphy. Gradation on a scale of the order of 400 m could not possibly result from processes of crystal sorting, and the upward modal and normative variations are interpreted in terms of crystallization along a four-phase cotectic becoming progresively more distant from clinopyroxene and olivine.

Crescumulate layers, developed only within the crescumulate zone, have been described earlier (Robins 1973). Layers are isomodal, pegmatitic and bounded by ratio, phase or form contacts. The crescumulate layers are generally concordant with adjacent layers of other types and often have planar bases and highly irregular tops (Fig. 8 A). Planar, discordant contacts cutting abruptly across well-layered cumulates are also present in places and suggest either an

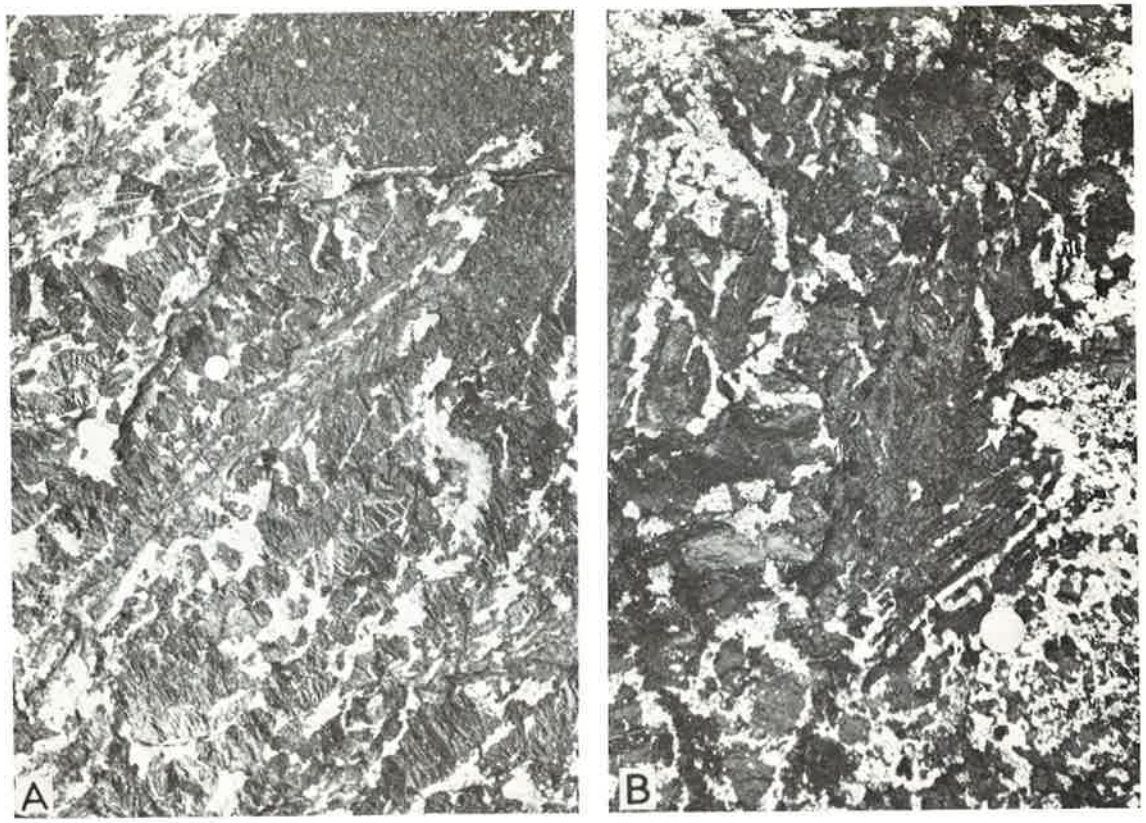

Fig. 8. (A) Highly-elongated skeletal olivines and elongated clinopyroxenes in a crescumulate layer. The irregular top of the layer at the upper right appears to have been buried beneath later cumulates. (B) Large skeletal olivine of relatively equant form in a crescumulate on Mjånes, Stjernøy (Fig. 1). The constituent plates are clearly parallel to potential crystal faces. The coin used for scale has a diameter of 2.5 cm.

origin as separate injections, as is the case for some of the Rhum harrisites (Harker 1908, Donaldson 1974, 1975) which the Rognsund crescumulates most closely resemble, or slumping of the adjacent cumulates.

The majority of the crescumulates are characterized by skeletal olivines; less commonly they contain olivine parallel-growth forms (Robins 1973, Fig. 1). Occasionally, both types of crystal are found within a single layer. The skeletal olivines may be very large and highly elongated. Some olivine crystals extend for up to 1 m from the base of a layer to its top (Fig. 8 A). In other layers the olivines are more equidimensional (Fig. 8 B), and resemble the very much smaller skeletal olivines from picritic minor intrusions figured by Drever & Johnston (1957). In these layers there is no systematic mineral orientation.

Orientated olivine is accompanied by pyroxene megacrysts which also may be elongated at a high angle to layer boundaries (Fig. 8 A). The olivines and pyroxenes of the crescumulates are invariably surrounded by poikilitic, unzoned plagioclase, probably of heteradcumulus origin. Subhedral, cumulus plagioclase has, however, been observed within pyroxenes in certain crescumulates.

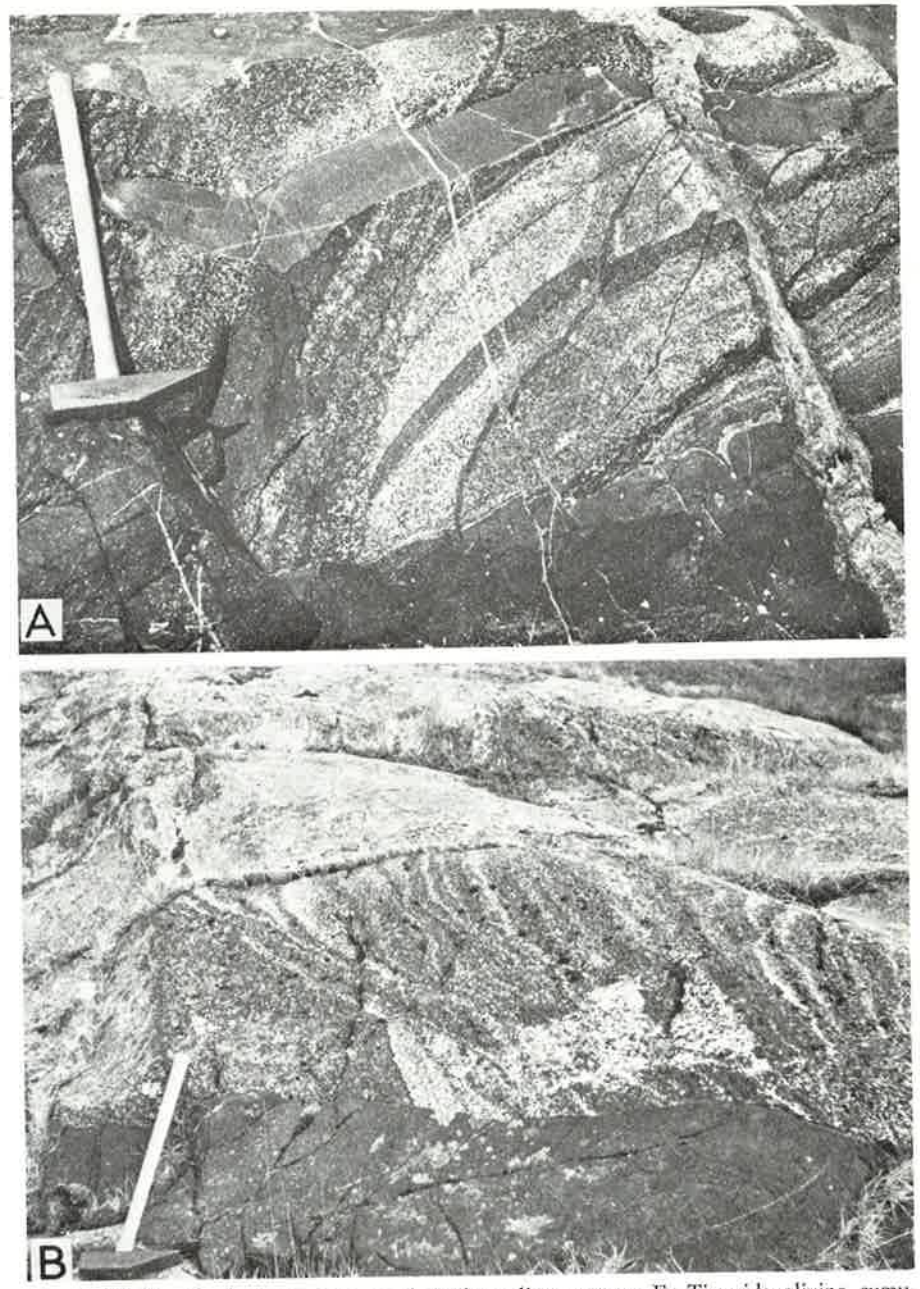

Fig. 9. (A) Erosional discordance in plagioclase–clinopyroxene–Fe–Ti oxide–olivine cumulates from the upper part of the cumulate zone. The rhythmic layering is cut by several generations of mafic dykes and by syenite pegmatites. (B) Erosional channel subsequently filled by mineral-graded clinopyroxene–plagioclase–Fe–Ti oxide–olivine cumulates at the base of the cumulate zone. In the foreground the rhythmic layering is cut almost at right-angles by a picritic dyke. Hammer-shaft is 60 cm long.

It has been argued that crescumulates originate by the rapid enlargement of cumulus crystals lying on the temporary floor of an intrusion due to immersion

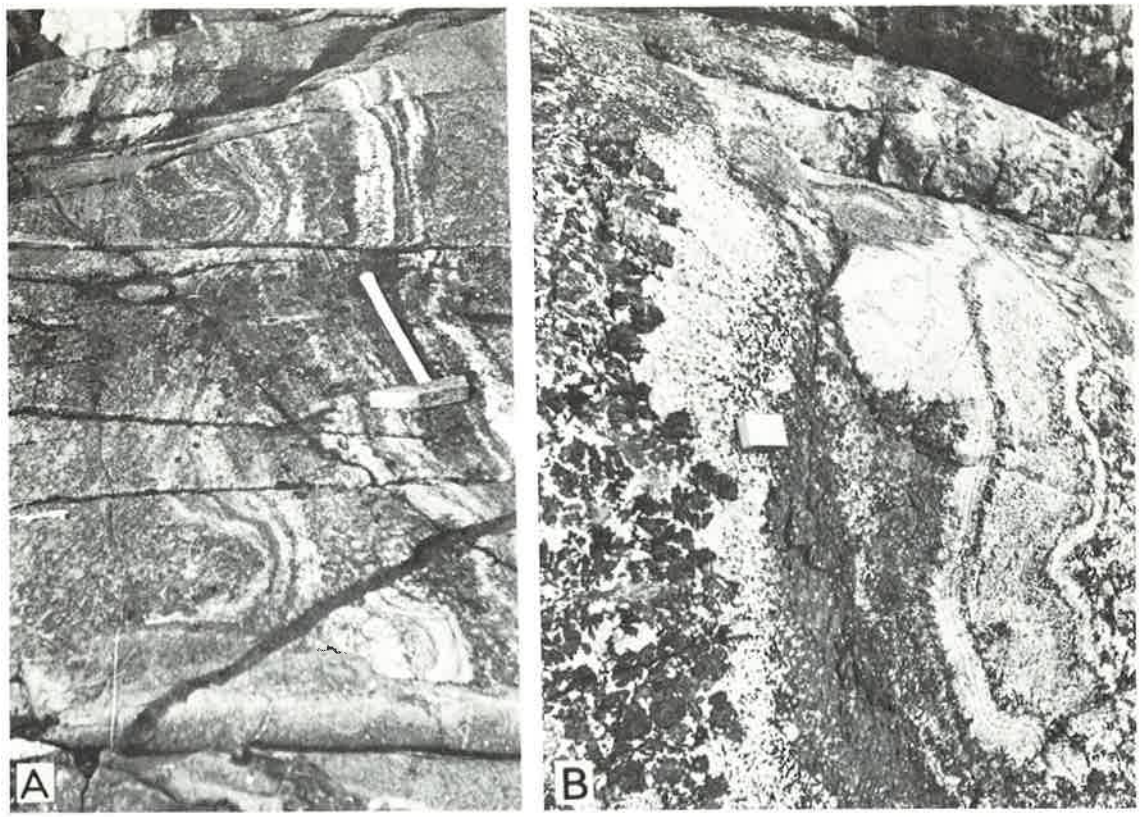

Fig. 10. (A) Load structures at the base of a layer of clinopyroxene–Fe–Ti oxide–olivine cumulate (left-hand side of figure) overlying plagioclase-rich cumulates. Hammer-shaft is 60 cm long. (B) Slump fold developed in adcumulate horizons within a crescumulate-zone sequence of varied composition. Layers young to the right. A matchbox measuring 5.5x3.5 cm gives the scale.

in a stagnant supersaturated magma (Wadsworth 1961, Robins 1973). Donaldson (1977) suggests that supersaturation may be due to heat conduction through the underlying cumulates, but their insulating effect on the magma makes this unlikely (Irvine 1970, 1979, Hess 1972, Huppert & Sparks 1980). Supersaturation may arise, if nucleation is inhibited, by the flow of a water-undersaturated magma into a region of higher pressure (Jackson 1961, Wager 1963, Irvine 1970), by cooler magma descending from the roof or walls of an intrusion (Hess 1960, Wager & Brown 1968), or by a sudden loss of volatiles (Donaldson 1974, 1975).

Erosional structures, principally small-scale discordances between layers, provide the most reliable evidence of stratigraphic sequence, and also give evidence of the action of magmatic currents of variable competence. Erosional bases to a layer, or groups of layers (Fig. 9 A), are of sporadic but fairly common occurrence, but it is only rarely that they can be related to larger structures such as erosional channels subsequently infilled by trough-shaped layers (Fig. 9 B).

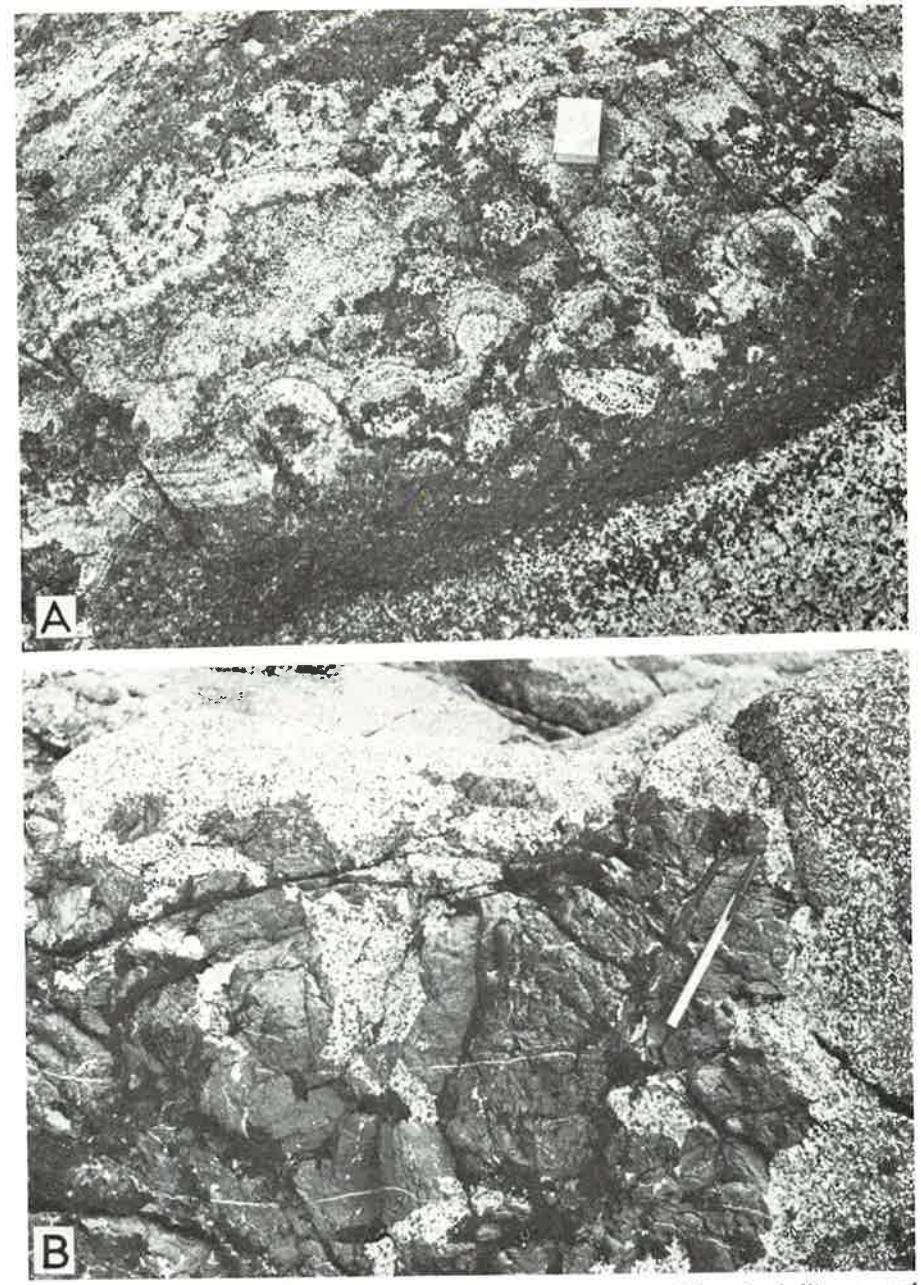

Fig. 11. (A) Structures resulting from the mobility of cumulates. Note the balling-up and partial disruption of the leucocratic layer and the injection of the underlying cumulate upwards (top left of figure). Matchbox employed for scale measures 5.5x3.5 cm. (B) Injection of slumped olivine, clinopyroxene crescumulate layer by temporarily remobilised plagioclase–clinopyroxene–olivine cumulate.

Load structures are infrequent but have been observed where dense clinopyroxene, olivine, Fe-Ti oxide cumulates overlie plagioclase-bearing cumulates of presumed ortho- or mesocumulate type, and where adcumulates rested upon

mobile ortho- or mesocumulates. In the former case, the overlying layer has bulbous downward protrusions resembling load casts, beneath which rhythmic layers are thinned (Fig. 10 A). Adcumulates residing on a mobile substratum became balled up and disrupted, while the underlying cumulate was injected upwards as dykes and mushroom-shaped bodies (Fig. 11 A). These structures may have a close genetic connection with slumping and resemble the squeeze up figured by Hess (1960).

Slump structures are particularly well developed in the upper part of the crescumulate zone at the northern extremity of its outcrop but elsewhere they are rare. Slumped, thinly-layered cumulates were folded (Fig. 10 B), and there is evidence that some cumulates were able to inject others (Fig. 11 B). During temporary remobilization, slump breccias were formed and consist of fragments originating from crescumulate and adcumulate layers enclosed within either homogeneous gabbro or a matrix with discontinuous and contorted layering.

The schlieren and irregular layers of eucritic or allivalitic composition observed in the olivine–clinopyroxene cumulates of the basal zone, may also have resulted from slumping of unstable crystal accumulations.

Autoliths of gabbroic composition are present in the cumulate zone, but are uncommon. They may be partly embedded in pre-existing cumulates and draped by later deposits (Fig. 12).

The amphibole–plagioclase pegmatites occur along a poorly exposed, laterally discontinuous zone maintaining a constant level within the basal zone; its thickness rarely exceeds 50 m. The zone consists of concordant comb-structured veins up to 30 cm wide separated either by form contacts or by thin and often deformed layers of variably saussuritized plagioclase, clinopyroxene, olivine cumulate in which large amphiboles are sporadically developed. Cross-cutting relationships between veins have not been observed, nor have the veins been seen to cut rhythmic layers.

The modal composition of the veins is highly variable: Some examples are oxide-rich hornblendites or pyroxene hornblendites but the majority are amphibole gabbros (bojites). All share a common structure, however, of bladed amphiboles, broadening and branching as they extend *from both margins* of the veins. Several veins contain laminated plagioclases partly or entirely enclosed in the margins of the amphiboles (Fig. 13).

The amphibole–plagioclase pegmatites bear a superficial resemblance to some crescumulates, such as the pyroxene crescumulates of the Skaergaard intrusion (McBirney & Noyes 1979, Plate 5 F), and were interpreted as such in an earlier account (Robins & Gardner 1974). However, in most crescumulates, as well as in related rocks showing 'Willow Lake' layering (Taubeneck & Poldervaart 1960) or 'comb' layering (Moore & Lockwood 1973), individual layers are asymmetrical and lack the bilateral structure of the Rognsund veins. In the

Fig. 12. Gabbro autolith impacted into pre-existing leucocratic cumulates (lowest part of figure) and buried by later deposits. Note that the leucocratic cumulates which are draped in a thin layer over the top of the autolith are absent along the 'overhang' beside the matchbox.

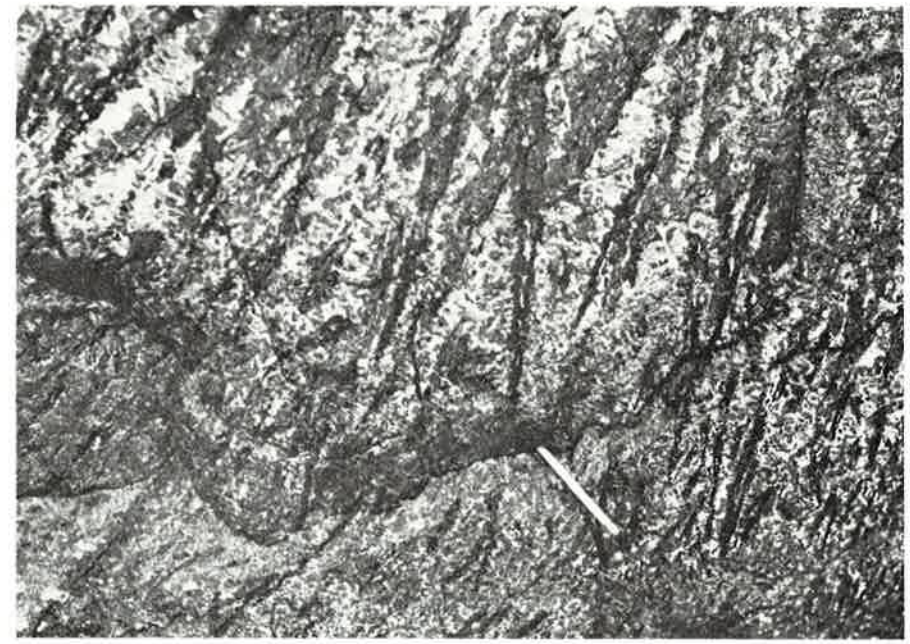

Fig. 13. Skeletal amphiboles, broadening and branching away from a vein margin in the basal zone. Note the laminated plagioclases within the margins of the amphiboles. Matchstick is 4.5 cm long.

Rhum harrisites, regarded by Wager & Brown (1968) as typical crescumulates, olivine crystals apparently grew downwards and laterally, as well as upwards (Donaldson 1974, 1975). In some occurrences, however, the harrisites have field relationships which suggest separate emplacement (Harker 1908, Donaldson 1975). The anorthite–hornblende pegmatites of the Duke Island Alaskan-type ultramafic complex (Irvine 1974) have the same internal structure as the Rognsund veins. They occur as parallel swarms and multiple dykes (Irvine 1974, Figs. 12 & 13, also Plate 43, Fig. 1 and Plate 44, Fig. 1) cutting all rocks of the complex and apparently replacing some. Comb-structured amphibole–plagioclase pegmatites are also known from other intrusions within the Seiland province, and have in many places strongly transgressive contacts with both layered gabbros and ultramafic rocks. These observations suggest that if the pegmatites are at all related to the Rognsund cumulates then they must result from the emplacement of volatile-enriched residual liquids in the form of sheets.

INTERPRETATION OF THE LAYERING

The cryptic mineralogical variation across the Rognsund intrusion shows that the layered series accumulated at the base of a magma chamber. The presence of structures resulting from current scouring, slumping and loading bear witness to the low degree of consolidation and high initial porosity of some of the cumulates, and their ability to flow and inject adjacent more competent cumulates. Hess (1960) estimated that cumulates at the base of the Stillwater intrusion were in a condition amenable to slumping to a depth of about 3 m below the temporary floor, whilst Irvine (1978) suggested that the Muskox cumulates were unconsolidated to depths of as much as 250 m. The processes by which these loosely compacted crystal mushes accumulated are presently under intense debate. In the elegant model intended to explain the density-graded layers and intervening homogeneous gabbros of the Skaergaard intrusion, Wager (1963) appealed to the settling of crystals from slow, steady convection currents and faster, intermittent currents resembling subaqueous turbidity currents. Both types of current were envisaged as sweeping from the roof down the steep walls of the magma chamber, where cooling and crystal growth was taking place, and spreading the suspended crystals over the temporary floor on which they could be sedimented (Wager 1963, Wager & Brown 1968). Support for the model is given by the similarities which exist between the structures exhibited by layered intrusions and clastic sedimentary sequences (Wadsworth 1973). The tendency for plagioclase to settle through basaltic magmas, in particular the Fe-rich magmas deduced to have existed in tholeiitic gabbro intrusions, has generally been considered to be slight but positive (Wager & Deer 1939, Wager & Brown 1968). However, calculations and experimental determinations of the densities of successive Skaergaard liquids (Bottinga & Weill 1970, Murase & McBirney 1973) show that plagioclase would almost certainly have floated throughout most of the fractionation history of the intrusion. A similar deduction has also been reached for the

Kiglapait intrusion (Morse 1979). Flotation of plagioclase has been demonstrated experimentally for a variety of basaltic melts (Campbell et al. 1978) and has been invoked as a major factor in the generation of anorthosites (Grout 1928, Olmsted 1968, Morse 1968, 1979).

The significance of the non-Newtonian properties of magmas (Shaw 1969) has been explored by McBirney & Noyes (1979). They suggest that the sizes and rates of growth of crystals in layered mafic intrusions were in general too small for crystal settling to be of significance in their origin. There is, however, a considerable body of observational evidence supporting the sinking of mafic phases even in rapidly-cooled basaltic lavas (Fuller 1939, Yagi 1965) and short-lived lava lakes (Richter & Moore 1966, Moore & Evans 1967, Evans & Moore 1968). Despite the evidence supporting the concept of plagioclase flotation in basaltic magmas, the relative thickness of gabbroic rocks formed by crystallization on the roof, walls and floors of major intrusions can leave no doubt as to the reality and importance of plagioclase accumulation at the base of basaltic magma chambers (Campbell 1978, Irvine 1979, 1980a, Morse 1979, McBirney & Noyes 1979). Suggested solutions to this paradox include settling of composite grains (Hess 1960, Campbell 1978), *in situ* crystallization (Campbell 1978, Morse 1979, McBirney & Noyes 1979) and various types of transport in density currents (Hess 1960, Wager & Brown 1968, Irvine 1980a). All of these probably play a part in the generation of cumulates in the various parts of mafic intrusions. Monomineralic layers, mineral lamination and lineation in layered intrusions are, however, difficult to explain either by the sinking of glomerocrysts or by *in situ* crystallization. The best explanation of lamination is probably still accumulation under the influence of magmatic currents, though it may also possibly arise by the re-orientation of tabular crystals during compaction. Lineation of grains within the plane of the rhythmic layering is even more difficult to understand without postulating magmatic circulation. Lineation has been reported relatively infrequently but detailed petrofabric studies of cumulates may show it to be more common than is generally appreciated (e.g. Fortey 1980). On the other hand, the long and delicate crystals of some crescumulates evidently sprouted up from the floor of the intrusion, and grew into motionless magma. The unorientated, equant olivines and pyroxenes of other crescumulates must have grown *in situ* from a stagnant zone of supersaturated magma immediately above the surface of the crystal mush. Heterogeneous nucleation possibly played an important part in the generation of both types of crescumulates.

Crescumulates and those layers which have been called adcumulates by Wager et al. (1960) behaved as relatively competent rocks during slumping. This suggests that both these types of cumulate were consolidated at an early stage in the gradual solidification of the cumulate pile (Hess 1960, Wadsworth 1973). It has been supposed that adcumulates have developed by enlargement of grains while they were still at the top of the cumulate pile, due to contact with supersaturated magma (Brown 1956, Hess 1960, Wager et al. 1960, Wager 1963). Diffusion in basaltic magmas may, however, be too sluggish for this to occur (Hess 1972). Grain-boundary configurations in some monomin-

eralic cumulates can suggest that crystals sintered together under the influence of interfacial tension (Voll 1960). Sintering is a process by which the packing of crystal aggregates in magma chambers can be increased under isothermal conditions (Kingery 1959).

The cyclicity of rhythmic layering may be interpreted in terms of either chemical or mechanical effects. Proponents of the *in situ* origin of cumulates direct attention towards cyclic nucleation and crystallization (Campbell 1978, Maaløe 1978, McBirney & Noyes 1979). Others have emphasized the role of convection in the intermittent transport of crystals to the floor of the magma chamber (Hess 1960, Wager & Brown 1968, Irvine 1979, 1980a) or in the double-diffusive stratification of a magma chamber (McBirney & Noyes 1979, Irvine 1980a, 1980b, Chen & Turner 1980). There are considerable difficulties with the application of hypotheses implying an *in situ* origin for all layer types; the variety of internal structures, mineralogical composition and textural relationships in layers argue for more complex interactions than seem to be possible in systems in which periodic supersaturation and crystal growth are the main active processes. The development of layers in the Rognsund intrusion is envisaged as a complex process involving episodes of *in situ* crystallization, in which crescumulates were generated from batches of stationary, supercooled magma, and episodes in which crystal suspensions in cooler magma moved over the floor of the intrusion beneath less dense magma. Suspensions may have arisen under the roof of the intrusion and descended in the teardrop manner suggested by Hess (1960), they may have been started by the remobilization of crystal accumulations near the base of sidewalls (Irvine 1980a), or may be due to the tapping of 'wall cells' by a descending boundary layer (Irvine 1980b). Plagioclase is envisaged as being entrained initially by the yield strength of the enclosing magma (Irvine 1980a) and later by a combination of subsequent density currents and crystallization, sintering and other related effects in the pore liquid. Experiments show that efficient sorting of dense minerals can result from settling over distances of as little as 2.5 m in suspensions containing crystals to the extent of 10–30% by volume (Campbell et al. 1978). Density-graded layers may represent settling of mafic minerals from bottom-hugging crystal suspensions after their emplacement, or sorting which took place during the downward flow of the suspensions. The coarse grain size of the Rognsund cumulates suggests the likelihood of relatively rapid settling for at least olivine and pyroxene.

Petrography

Primary microtextures are poorly preserved in the Rognsund intrusion. Most samples show tectonite or metamorphic fabrics, and the primary minerals are often represented by porphyroclasts. In multiphase cumulates, the cumulus or inter-cumulus status of individual minerals is generally difficult to assess, and detailed classification of assemblages in terms of ortho-, meso-, ad- and heterad-cumulate processes is rarely possible. Metamorphic parageneses range in character from those typical of the granulite facies to those developed in the greenschist facies. Metamorphic reconstitution caused the disappearance of some minor phases from the mode, exsolution of high-temperature solid solutions, textural reorganization, and secondary zonation of some relict igneous minerals.

PRIMARY TEXTURES

The layered series was composed of the following primary minerals combined in various proportions: plagioclase, Ca-rich clinopyroxene, olivine, magnetite$_{ss}$, ilmenite and hercynitic spinel. Olivine was absent from the contaminated zone, being proxied by orthopyroxene which is accompanied by apatite and possibly amphibole in addition to the minerals listed above.

The contaminated zone. The main rock type in this zone is a coarse-grained feldspar–phyric metagabbro or feldspar–blastoporphyritic amphibolite with very subordinate amounts of clinopyroxene–phyric metagabbro. Against the external contact of the zone, the metagabbros are fine-grained and generally have granular textures, though plagioclase phenocrysts are occasionally observed. This fine-grained facies is interpreted as a marginal chill.

Plagioclase usually occurs as large deformed relics showing strong normal zoning, enclosed by a foam-textured mosaic of smaller and more sodic metamorphic plagioclase. Ca-rich clinopyroxenes and the oxide phases are extensively replaced at grain boundaries against plagioclase by a dark brown amphibole. Unreplaced cores are characterized by exsolved orthopyroxene lamellae parallel to (100). Strongly pleochroic orthopyroxene is present in subordinate amounts, except in the chilled metagabbros adjacent to the margin of the intrusion where it has a mode equal to that of clinopyroxene and contains exsolution lamellae of Ca-rich pyroxene. In the chill, brown amphibole is present; it forms large plates poikilitically enclosing the other phases.

The layered series. The two lowermost zones of the layered series are dominated by melanocratic clinopyroxene, olivine, plagioclase cumulates. The lowest members of the basal zone in the vicinity of Skarvvand (Plate 1), are mainly composed of clinopyroxene–olivine orthocumulates, containing subhedral, zoned cumulus phases poikilitically enclosed in much larger plagioclases. The brownish or mauve clinopyroxenes are distinguished from those of the contaminated zone by their characteristic sagenitic structure. They are crowded with thin plates of green spinel and brown ilmenite (Fig. 14) which are orientated in several different directions, concentrated in concentric zones, and usually absent from the margins of the pyroxenes. These may, however, be accompanied by limited amounts of exsolved Ca-poor pyroxene as short lamellae parallel to (100). The latter are free from spinel and ilmenite plates, but may contain distinct grains of these phases. Thin plates are also generally absent in narrow haloes around the orthopyroxene lamellae, which are characterized by tiny transverse fractures. Fracturing was probably induced during cooling by a

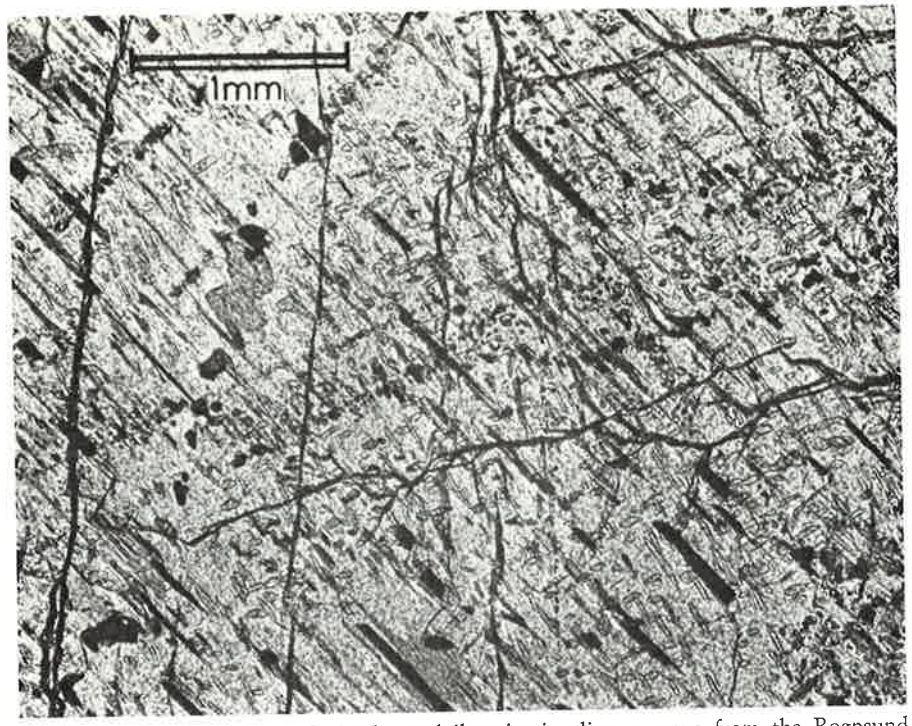

Fig. 14. Typical exsolution of picotite and ilmenite in clinopyroxene from the Rognsund intrusion.

higher coefficient of expansion than the host (Skinner 1966). Grains of spinel and ilmenite with plate-free haloes, concentrated along certain bands crossing clinopyroxenes at various angles, suggest migration of the exsolved minerals.

Three-phase cumulates from the basal zone carry large strained plagioclase laths with complex twinning on Carlsbad, albite, pericline and acline laws. Normal zoning is often present but is usually spatially related to metamorphic amphibole. Cumulus plagioclase is also generally surrounded by a more sodic generation of granular metamorphic plagioclase.

The amphibole–plagioclase pegmatites within the upper part of the basal zone are olivine-free. They contain highly-elongated brown amphibole with simple twins on (100), poikilitically enclosing irregular clinopyroxenes and Fe-Ti oxides and subophitically surrounding strongly-zoned and often highly-deformed plagioclase laths. The latter may define a lamination orientated at high angles to the direction of amphibole elongation. Gabbroic layers between the pegmatites appear to have orthocumulate textures. Cumulus olivine in these is represented by orthopyroxene–magnetite symplectites, and fairly abundant magnetite, containing exsolved hercynite and ilmenite, occurs as an intercumulus phase together with separate ilmenites. Amphibole in the cumulates appears to be porphyroblastic.

Except for their equant feldspars, the three-phase cumulates of the crescumulate zone are similar to those of the basal zone. Above the crescumulate/

cumulate zone boundary, cumulus oxides appear and give rise to distinctive textures. Clinopyroxene–olivine–oxide cumulates are texturally well-preserved, containing subhedral and occasionally laminated clinopyroxenes which are enclosed in a matrix of oxides, including magnetite, polysynthetically twinned ilmenite and hercynite. Small euhedral to subhedral grains of oxides included in the clinopyroxenes prove the cumulus nature of magnetite and ilmenite. Little olivine remains after oxidation or reaction with plagioclase. Hercynite is invariably associated with magnetite, probably due to the high-temperature breakdown of a magnetite–hercynite solid solution. Hercynite lamellae parallel to (100) are abundant in magnetite, which also contains infrequent, thin lamellae of ilmenite parallel to (111). Hercynite grains were also exsolved along primary magnetite–ilmenite grain boundaries; later migration of the grain boundaries due to addition of ilmenite exsolved from magnetite, left the spinel grains isolated in ilmenite. Breakdown of the magnetite solid solution also gave rise to warts of ilmenite–hercynite symplectite extending from magnetite–ilmenite grain boundaries into magnetite. Ilmenite contrasts with magnetite in containing few exsolved lamellae of spinel or magnetite. These textural relationships are also typical of inter-cumulus oxides in the basal and crescumulate zone.

Average cumulates in the cumulate zone have rarely escaped extensive textural changes during subsequent deformation and metamorphism. The preserved textures are similar to those of the three-phase cumulates of the basal zone with the exceptions that oxides are generally more abundant and their cumulus origin is illustrated by the poikilitic inclusion of euhedral or subhedral crystals within the other cumulus phases.

Sulphides are present in very small amounts in nearly all cumulates of the Rognsund intrusion. Pyrrhotite, either as homogeneous grains or containing exsolved pentlandite, is the dominant sulphide species. Chalcopyrite, pyrite, sphalerite and covellite also occur in minor amounts in some rocks.

METAMORPHIC TEXTURES

Transformation of the primary paragenesis can be subdivided into three episodes: Deformation and syntectonic recrystallization; High-temperature annealing recrystallization; Subsequent retrogressive metamorphism in the amphibolite and greenschist facies.

Deformation is exhibited by all of the main mineral species. Plagioclases were most strongly affected, being strained, kinked or folded. Deformed crystals of plagioclase and clinopyroxene show strain-induced twinning, while deformation lamellae may be present in olivine. Along zones of strong shearing, primary minerals were broken down and recrystallized into granular aggregates of smaller deformed crystals which are compositionally similar to their parents.

Deformation and recrystallization has generally resulted in a foliation defined by lenticular aggregates of recrystallized grains, cored by porphyroclasts derived from the primary phases. The foliation generally closely parallels the

Fig. 15. Folded mineral-graded layers cut by an axial-planar foliation. Metamorphic fabrics in the Rognsund intrusion are generally parallel to the primary rhythmic layering.

relict rhythmic layering, but may occasionally be at an angle to it and axial planar to small-scale open folds (Fig. 15).

Annealing recrystallization began at high temperature and continued as the temperature waned into the almandine–amphibolite facies. Plagioclase recrystallized with the production of foam-textured, strain-free, zoned grains smaller in size than the parent deformed crystals. Compositionally, the new generation of plagioclase is usually more sodic than the cumulus crystals, lying in the labradorite–bytownite range. Zonation is generally normal but reverse zoning is occasionally observed. In one sample from the basal zone showing reverse zonation, a core composition was determined as An_{64} by universal-stage measurement of extinction angles in the zone normal to (010), while the margin was An_{69}. Many of the metamorphic feldspars in this sample contain fine striations or lamellae apparently of a second plagioclase feldspar; lamellae are restricted to the calcic margin in the zoned grain mentioned above, suggesting that the feldspars are Huttenlocher intergrowths (Smith 1974, p. 477).

Olivine reacted with plagioclase along mutual grain boundaries during annealing. The reaction products are generally warts or coronas of bronzitic orthopyroxene–clinopyroxene–hercynitic spinel symplectite. In detail the structure of the coronas is variable and complex. The branching of the interpenetrating pyroxenes and spinel grains in the symplectites suggests they could grow at the expense of either plagioclase or olivine, or both. A rim of spinel-

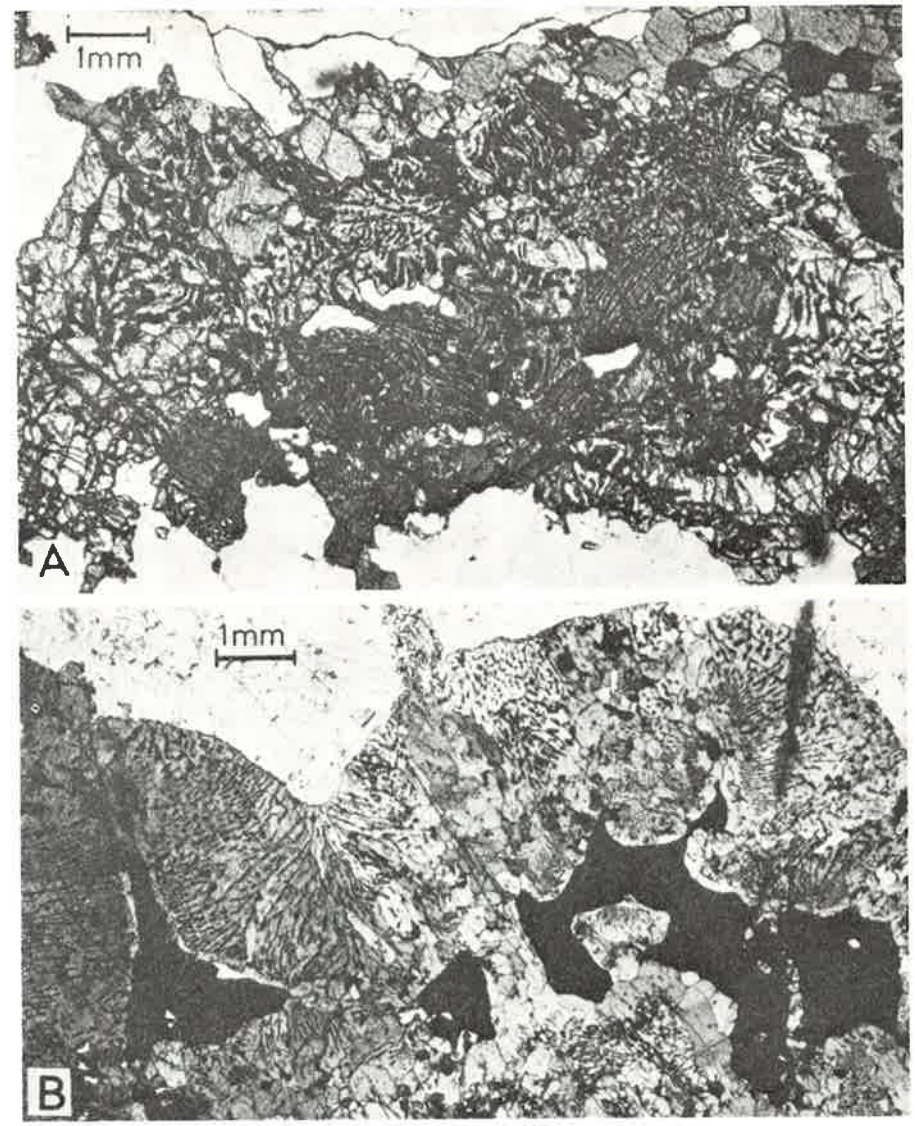

Fig. 16. (A) Orthopyroxene–magnetite/ilmenite symplectite produced by oxidation of an olivine relic from previous subsolidus reaction with plagioclase represented by the pyroxene–aluminous spinel symplectites. (B) Amphibole–aluminous spinel symplectite developed at plagioclase–Fe–Ti oxide and plagioclase–hercynitic spinel grain boundaries during amphibolitization of deformed cumulates.

free orthopyroxene or clinopyroxene usually separates olivine from the pyroxene-spinel symplectite and the interlamellar spacing in the symplectite decreases in the direction of growth (Gardner & Robins 1974) probably due to reaction under progressively lower temperatures (Chadwick 1972). In many plagioclase-rich cumulates, reaction has proceeded to completion, former olivine being pseudomorphed by pyroxene-spinel symplectites or by granular spinel-free pyroxene surrounded by symplectite. Small grains of Ca-rich pyroxene

clouding plagioclase in some coronites are believed to have originated in connection with the reaction between olivine and plagioclase.

In those rocks in which olivine was incompletely consumed by reaction with plagioclase, either because of limited amounts of the latter, or arrest of the reaction process, oxidation could occur. The product of oxidation is a lamellar orthopyroxene–magnetite/ilmenite intergrowth or vermicular symplectite (Fig. 16 A), which appears in places to have been subsequently recrystallized to patches of equigranular, subhedral orthopyroxene with interstitial Fe-Ti oxides and spinel. The occurrence of ilmenite in the intergrowths, the aluminous orthopyroxene and the exsolution of spinel lamellae from the magnetite suggests that exchange with other phases took place during the oxidation of olivine.

During annealing, some primary clinopyroxenes were recrystallized to a limited degree. Both primary and recrystallized grains exhibit extensive exsolution of spinel and ilmenite but this is absent from corona pyroxenes and pyroxenes clouding plagioclase. This may suggest that exsolution preceeded the reaction between olivine and plagioclase.

Subsequent metamorphism is evidenced by the widespread amphibolitization of the Rognsund intrusion. Brown amphiboles were generated by reaction at grain boundaries of plagioclase with clinopyroxene, Fe-Ti oxides and hercynitic spinel. Particularly in two latter cases, aluminous spinel was also a reaction product, giving rise to symplectitic coronas (Fig. 16 B). Continuing metamorphism at lower temperatures is reflected texturally by the crystallization of green amphiboles. The brown amphibole-spinel symplectites after clinopyroxene and plagioclase are replaced by green amphibole accompanied by epidote and, occasionally, biotite. The pyroxene in symplectites with spinel was also replaced by green amphibole, and the spinel by (?) diaspore. Olivine remaining after reaction with plagioclase and oxidation is sometimes represented by anthophyllite.

Plagioclase in certain samples is irregularly replaced by scapolite, and, particularly adjacent to joints and amphibole–plagioclase pegmatites, by albite heavily dusted with calcite, and porphyroblastic epidote. The mafic minerals in albite-bearing rocks are largely replaced by chlorite, anthophyllite and minor biotite.

Primary mineralogy

The compositions of the cumulus silicate minerals of the Rognsund intrusion have been investigated by Universal–Stage optical techniques and electron microprobe micro-analysis. Derived compositional data are summarized and plotted against stratigraphic position in Fig. 4.

PLAGIOCLASE

Plagioclase compositions were estimated in nineteen thin-sections from extinction angles in the zone normal to (010) employing the Universal–Stage. Extinc-

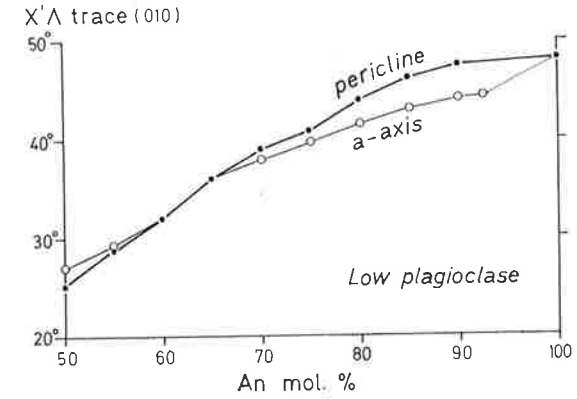

Fig. 17. Determinative curves for low-plagioclase based on extinction angles in the zone normal to (010) and in the direction of the pericline twin lamellae. The pericline curve was constructed using values from Smith (1974) and optic migration curves of Burri et al. (1967). The a-axis curve is from Smith (1974).

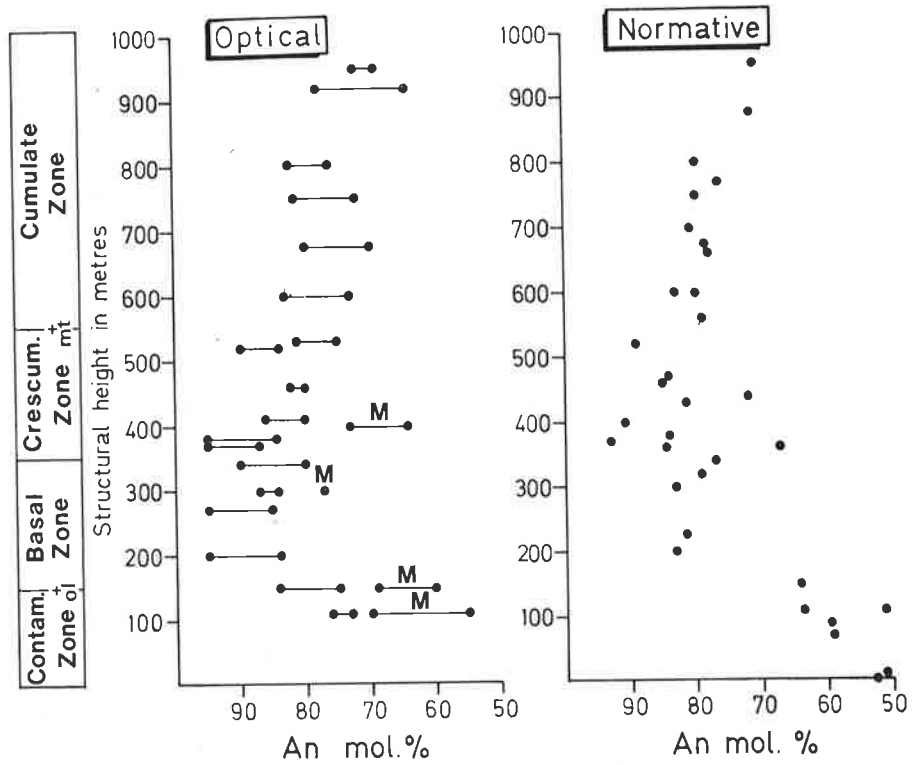

Fig. 18. Variation of optically–determined plagioclase compositions in the Rognsund intrusion (points give maximum and minimum anorthite contents for each sample) compared with the normative composition of plagioclase from whole-rock analyses (including ne recalculated to ab). M refers to plagioclases belonging to the metamorphic generation.

tion angles in the a-axis section were translated into %An using the curve for low plagioclase constructed by Smith (1974, p. 404) from the data of Burri et al. (1967). The majority of extinction angles were measured, however, in sections at right-angles to the pericline twin lamellae. In this case, compositions were estimated from a new curve (Fig. 17) constructed by the Biot–Fresnel

Table 2. Arithmetic means of microprobe analyses of plagioclases

Sample no.	109SD	37SD	29SD	33SD	25SF	30SD	28SD
Strat.pos.	150 m	300 m	550 m	600 m	700 m	800 m	950 m
n =	9	10	10	12	10	9	9
SiO_2	47.49	47.35	49.00	48.67	49.10	49.95	52.08
Al_2O_3	33.60	33.90	32.36	32.91	32.59	31.48	29.69
CaO	16.97	17.30	16.42	16.09	16.60	14.81	13.37
Na_2O	1.75	1.68	2.03[1]	2.37	2.02[1]	2.89	3.99
K_2O	0.08	0.07	0.18	0.07	0.09	0.09	0.10
TOTAL	99.99	100.31	99.99	100.11	100.40	99.20	99.24
Cations to 32 (0)							
Si	8.724	8.673	9.028	8.892	9.013	9.174	9.573
Al	7.261	7.299	7.028	7.096	7.050	6.814	6.395
Ca	3.339	3.397	3.235	3.150	3.262	2.915	2.621
Na	0.622	0.596	0.725	0.828	0.718	1.013	1.405
K	0.019	0.016	0.040	0.015	0.020	0.020	0.022
Z	15.985	15.972	16.056	15.988	16.063	15.988	15.932
X	3.980	4.009	4.000	3.993	4.000	3.948	4.047
An%	83.9	84.7	80.9	78.9	81.6	73.8	64.8
Range	85.6–83.6	87.6–81.2	84.8–79.3	81.4–74.7	89.3–77.4	80.2–70.4	69.1–61.9

[1]) Low analytical values adjusted such that X = 4.000.

method on the basis of sigma values quoted by Smith (1974), and the optic migration curves of Burri et al. (1967). Results of these methods were checked in certain cases by Universal–Stage conoscopic determinations of 2V, employing the low-plagioclase curve of Smith (1958).

The optical determinations suggest that both relict primary plagioclase and metamorphic plagioclases have quite wide ranges of composition in each sample. In some cases the compositional variations are bimodal, with the metamorphic plagioclases being more sodic than the relict cumulus crystals. The relict plagioclases of the basal and crescumulate zones generally fall into the calcic–bytownite-sodic anorthite range, while those of the cumulate zone are sodic bytownite or labradorite (Fig. 18). Contaminated zone cumulus feldspars are also sodic bytownites; two sets of determinations suggest that they may become more calcic upwards in the cumulate stratigraphy. Within the layered series proper, the compositional ranges occupied by the relict cumulus feldspars are displaced to more sodic compositions as the sequence is ascended. This trend is paralleled by normative plagioclase compositions derived from major-element analyses of average cumulates (Fig. 18) and is considered a true reflection of the primary cryptic layering.

Electron microprobe analyses of relict cumulus plagioclases have been carried out on seven samples (Table 2). The most calcium-rich feldspars analysed are calcic bytownites similar in composition to the most basic plagioclases which crystallize from common intrusive basaltic magmas (Brown 1967, Wager 1968). With the exception of one sample (33 SD), mean plagioclase composi-

Table 3. Arithmetic means of microprobe analyses of clinopyroxenes

Sample no.	38SD	36SD	86SD	648	33SD	32SD	25SF	30SD	28SD	T4.4
Strat.pos.	200 m	400 m	430 m	500 m	600 m	675 m	700 m	800 m	950 m	x
n =	3	4	8	9	7	9	4	9	10	1
SiO_2	50.33	50.73	48.25	48.57	49.62	49.83	48.95	49.98	49.96	50.30
TiO_2	0.62	1.00	1.21	1.17	0.95	1.05	0.78	0.77	1.10	0.59
Al_2O_3	5.50	4.48	7.04	6.97	5.69	5.08	5.12	5.57	5.76	5.00
Cr_2O_3	0.33	0.30	n.d.	n.d.	n.d.	n.d.	n.d.	n.d.	n.d.	n.d.
FeO	4.95	5.32	6.39	6.61	7.58	8.03	8.53	8.55	8.94	8.51+
MnO	0.13	0.13	0.12	0.13	0.15	0.18	0.24	0.20	0.17	0.20
MgO	14.65	14.12	13.62	13.51	12.74	14.00	12.67	11.74	11.49	12.60
CaO	21.73	23.03	21.86	22.33	22.16	22.27	22.39	22.30	22.23	21.00
Na_2O	0.89	0.82	0.84	0.70	0.66	0.77	0.74	0.73	1.04	1.00
TOTAL	99.13	99.99	99.33	99.99	99.55	101.21	99.43	99.84	100.69	99.91
Cations to 6 (0)										
Si	1.869	1.879	1.802	1.803	1.854	1.841	1.846	1.870	1.858	1.862
Al^4	0.131	0.121	0.198	0.159	1.146	0.159	0.154	0.130	0.142	0.138
Al^6	0.110	0.074	0.113	0.109	0.105	0.062	0.074	0.116	0.110	0.080
Ti	0.018	0.029	0.034	0.033	0.027	0.030	0.022	0.022	0.031	0.044
Fe^{2+}	0.153	0.165	0.199	0.205	0.237	0.247	0.269	0.268	0.278	0.264[z]
Mn	0.003	0.003	0.003	0.003	0.005	0.006	0.008	0.006	0.006	0.007
Mg	0.811	0.780	0.757	0.748	0.709	0.770	0.715	0.655	0.637	0.694
Ca	0.864	0.913	0.874	0.888	0.887	0.880	0.907	0.894	0.886	0.832
Na	0.062	0.059	0.060	0.049	0.048	0.052	0.052	0.053	0.075	0.071
WXY	2.021	2.023	2.040	2.035	2.018	2.045	2.045	2.014	2.023	1.992
Al_z%	6.77	6.25	9.97	9.85	7.30	8.05	7.68	6.52	7.11	6.90
Ca	47.16	49.07	47.64	48.14	48.26	46.25	47.78	49.05	49.04	48.33
Mg	44.23	41.86	41.29	40.52	38.60	40.44	37.61	35.92	35.26	37.14
Fe	8.61	9.07	11.08	11.34	13.14	13.31	14.61	15.03	15.69	14.52

n.d. = not determined

x = Spectrochemical analysis of separated clinopyroxene (Oosterom 1963), SiO_2 calculated by difference

\+ = Includes 1.9% Fe_2O_3

z = Includes 0.053 Fe^{3+}

tions vary systematically with position in the cumulate stratigraphy, from An_{85} in the basal zone to An_{65} close to the upper limit of the exposed cumulate zone. The compositional variations in each of the analysed samples are believed to be primary in origin or the result of partial re-equilibration during metamorphism.

PYROXENE

Analysed relict cumulus clinopyroxenes range from diopside in the basal zone and lower part of the crescumulate zone to salite in the rest of the layered series (Table 3). Their content of FeO increases regularly, and MgO decreases, with height in the cumulate sequence. CaO does not show a regular trend with height. Each of the analysed pyroxenes, however, contains more than 45 cation% Ca+Na, and they are, therefore, considerably richer in calcium than Mg-rich clinopyroxenes precipitated from intrusive tholeiitic magmas. Plotted

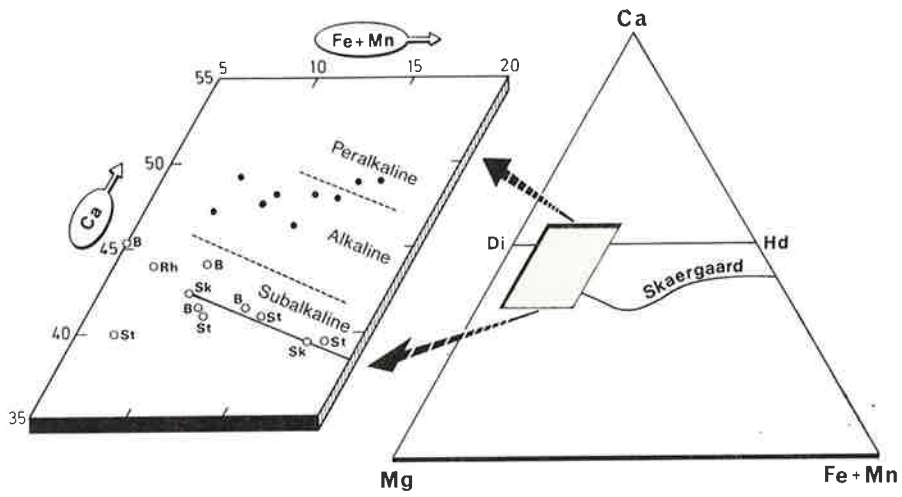

Fig. 19. Electron microprobe analyses of relict cumulus diopsides and salites plotted in the pyroxene quadrilateral. Fields for pyroxenes from different magma types are after Le Bas (1962). Sk, B, St and Rh refer to early Ca-rich pyroxenes from the Skaergaard, Bushveld, Stillwater and Rhum intrusions.

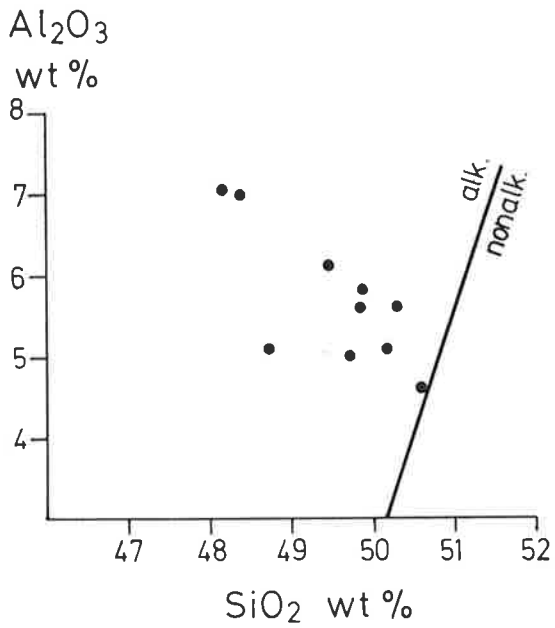

Fig. 20. Variation of Al_2O_3 in microprobe analyses of Rognsund intrusion Ca-rich pyroxenes with SiO_2. Fields for pyroxenes from alkaline and non-alkaline rocks are after Challis (1965).

in the pyroxene quadrilateral, mean analyses fall into the field for groundmass Ca-rich pyroxenes from alkaline lavas (Le Bas 1962) (Fig. 19).

Compared with Ca-rich clinopyroxenes from layered intrusions known to be of tholeiitic affinity, those from the Rognsund intrusion are abnormally rich in Al_2O_3, though not appreciably different in terms of TiO_2. Al_2O_3 in individual analyses has a negative correlation with SiO_2 (Fig. 20) suggesting that the

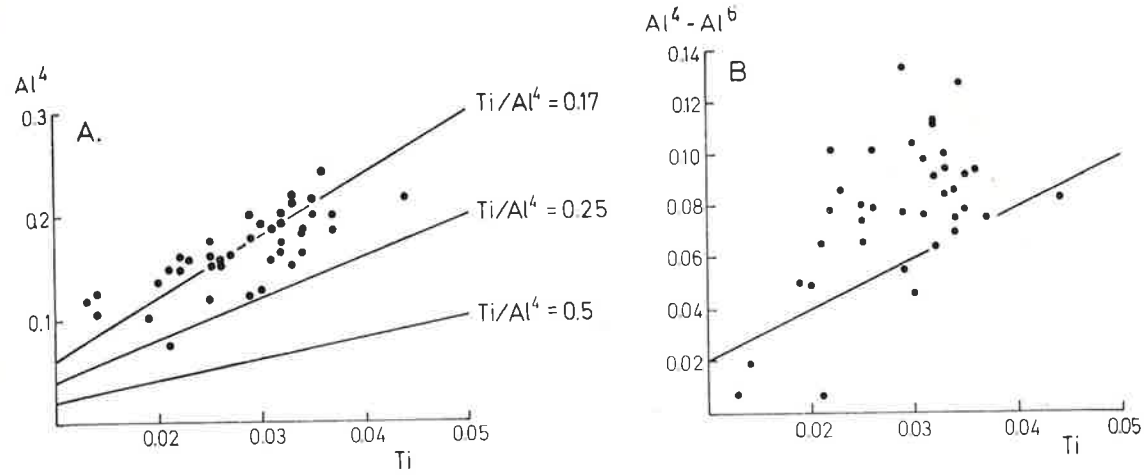

Fig. 21. Variation in Ti in the structural formulae of analysed Ca-rich pyroxenes with A: total tetrahedral Al, and B: tetrahedral Al in excess of that required for Ca-Tschermaks molecule.

majority of Al is located in tetrahedral sites. Al_z (= 100 $Al^4/2$) reaches values as high as 12% in extreme cases, and rarely falls below 6%. Al_z in low-pressure pyroxenes has been related to magma chemistry by Le Bas (1962) and Challis (1965), increasing undersaturation favouring replacement of Si by Al.

The relationship between Ti/Al^4 and Ti/Al^4–Al^6 (Fig. 21) indicates that the substitution of Ti in M1 sites is only about one-sixth of the Al substitution of Si, and that the excess of Al^4 relative to the amount required for Ca–Tschermaks molecule is generally above that necessary for formation of the titanpyroxene molecule. It seems probable that the excess Al^4 is balanced by chromium, trivalent iron or sodium. The mean chromium content of analysed clinopyroxenes from two samples collected low in the cumulate stratigraphy is 0.3% Cr_2O_3, while a clinopyroxene from the Stjernøy segment of the Rognsund gabbro analysed by spectrophotometric techniques (Oosterom 1963) contained 1.9 wt.% Fe_2O_3. In the structural formula, Fe^{3+} in the latter is similar in amount to, but slightly less than, Na (Table 3). The preliminary conclusion is that excess Al^4 is mainly balanced by Cr^{3+} and to a lesser degree by Na^+.

Plotting Al_2O_3 against an iron-magnesium ratio reveals that with fractionation, the pyroxenes first become rapidly enriched in alumina; this is followed by a sharp fall in the alumina content after which Al_2O_3 remains fairly constant. A similar, though more scattered pattern is shown by plotting TiO_2 against the same fractionation index (Fig. 22). All points with 100 (Fe + Mn/Mg + Fe + Mn) ratios lower than approximately 23 represent analyses from four samples from the basal and crescumulate zones, suggesting that the sudden decrease in Al_2O_3 and TiO_2 is connected with the beginning of magnetite and ilmenite crystallization. Similar patterns to those displayed in Fig. 22 have been described for zoned Ca-rich pyroxenes from the Shiant Sill (Gibb 1973), the

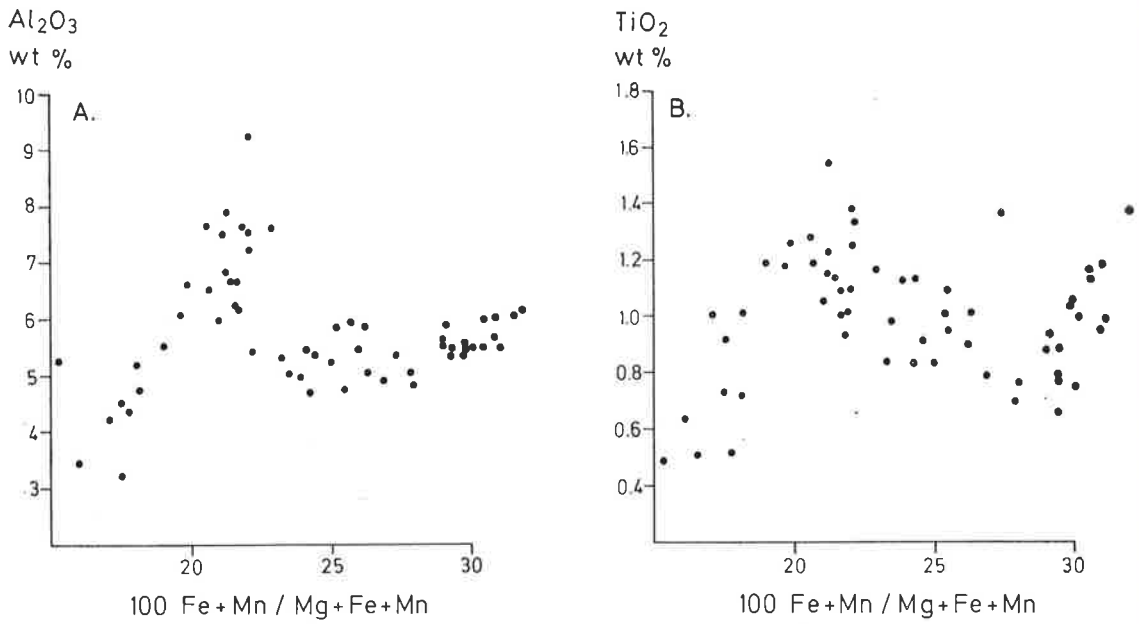

Fig. 22. Relationship of Al_2O_3 and TiO_2 in Ca-rich pyroxenes from the Rognsund intrusion to a fractionation index which correlates with position in the cumulate stratigraphy.

change from enrichment to depletion in Al and Ti taking place at an Fe/Mg + Fe ratio of approximately 0.35. The present data support the explanation preferred by Gibb (1973), viz: fractionation of olivine, clinopyroxene and plagioclase led to increase of Ti and Fe^{3+} activities in the liquid, Ti entering pyroxene in progressively greater amounts as titanpyroxene molecule. On the appearance of titaniferous magnetite and ilmenite, substitution of Ti in pyroxene was inhibited. There is, however, no clear pattern of Na_2O variation with iron ratio in the Rognsund pyroxenes, such as could be ascribed to variations in Fe^{3+} activity in the parent liquids (Gibb 1973). Na_2O varies irregularly, with concentrations ranging from 0.6 wt.% to an extreme of 1.2 wt.%, appreciably higher than those characteristic of low-pressure tholeiitic Ca-rich pyroxenes ($Na_2O<0.4\%$, Wilkinson 1974).

Exsolved plates of a green spinel, although volumetrically of little significance, are a ubiquitous and unusual feature of the pyroxenes from the Rognsund intrusion (Fig. 14). Microprobe analysis carried out on the wider plates of one pyroxene (Table 4) shows them to consist of picotite (Al>Cr, Fe/Mg = 2.2; Deer et al. 1962). Spinel lamellae are not uncommonly observed in pyroxenes from alpine peridotites (e.g. Warnaars 1967, Dickey 1970) and nodules in basaltic rocks (Le Maitre 1962, White 1966, Lovering & White 1969, Chapman 1975). They have also been reported in both the Ca-poor and Ca-rich pyroxenes of the Gosse Pile layered intrusion (Moore 1971). Spinel exsolution is often interpreted as due to the decomposition of moderate-pressure Al-rich pyroxenes.

Table 4. Electron microprobe analyses of exsolution lamellae in clinopyroxene

Sample no.	38SD				30SD
Mineral	Opx		Sp		Il
n =	5		3		4
SiO_2	55.43		n.d.		0.05
TiO_2	0.12		n.d.		48.23
Al_2O_3	1.88		40.92		0.05
Cr_2O_3	n.d		15.62		n.d.
FeO	15.14		35.56		47.01
MnO	0.31		0.54		0.53
MgO	26.94		6.65		1.39
CaO	0.45		n.d.		0.51
Na_2O	0.02		n.d.		0.02
TOTAL	100.29		99.29		97.79
Cations to 24 (0)					
Si	7.921		–		0.009
Ti	0.013		–		7.367
Al	0.317		8.623		0.012
Cr	–		2.207	12.0	–
Fe^{3+}			1.169		1.240
Fe^{2+}	1.810		4.147		6.747
Mn	0.038		0.082	6.0	0.092
Mg	5.737		1.772		0.421
Ca	0.070		–		0.111
Na	0.007		–		–
Ca	0.91	FeO	27.74		39.68
Mg	74.95	Fe_2O_3	8.69		8.06
Fe	24.14	Total	100.16		98.52

Opx = orthopyroxene; Sp = spinel; Il = ilmenite
n.d. = not determined

Spinel and ilmenite analyses were recalculated on the basis of 18 and 16 cations respectively, sufficient Fe^{3+} being calculated to bring the number of oxygens in the structural formula to 24.

Plates of an opaque mineral generally accompany the spinel, and are especially abundant in the more iron-rich pyroxenes of the cumulate zone; their low reflectance, optical anisotropy and an electron microprobe analysis (Table 4) shows them to be ilmenite.

Thin discontinuous orthopyroxene lamellae have been observed in some clinopyroxenes from the Rognsund intrusion (Table 4), but are rare. The high calcium of the Rognsund clinopyroxenes relative to those of common layered intrusions cannot, however, be related to such exsolution, that is, the analysed and plotted clinopyroxenes do not show a subsolidus trend. Comparison of the microprobe analyses presented here with spectrochemical analyses of *separated* clinopyroxenes published by Oosterom (1963), particularly that separated from sample T4.4 collected from the Stjernøy segment of the Rognsund intrusion (Table 3), reveals no significant differences. Exsolution of Ca-poor pyroxene from the Rognsund pyroxenes is too sporadic and too limited in volume to be

Table 5. Arithmetic means of electron microprobe analyses of olivines

Sample no.	38SD	37SD	36SD	86SD	648	66SF
Strat.pos.	200 m	300 m	400 m	430 m	500 m	770 m
n =	9	9	9	9	9	6
SiO_2	38.53	38.00	37.81	38.74	39.27	37.49
CaO	n.d.	n.d.	n.d.	0.02	0.01	0.01
FeO	23.30	23.22	23.37	24.26	23.63	30.62
MnO	0.46	0.45	0.44	0.27	0.33	0.53
MgO	38.02	38.20	38.30	36.90	37.85	32.21
NiO	n.d.	n.d.	n.d.	0.13	0.10	0.05
TOTAL	100.31	99.87	99.92	100.32	101.20	100.91
Cations to 4 (0)						
Si	1.004	0.995	0.991	1.012	1.013	1.006
Ca	–	–	–	0.000	0.000	0.000
Fe	0.508	0.509	0.512	0.530	0.510	0.687
Mn	0.010	0.010	0.010	0.006	0.007	0.012
Mg	1.475	1.491	1.496	1.437	1.455	1.288
Ni	–	–	–	0.003	0.002	0.001
$(Y)^6$	1.993	2.010	2.018	1.976	1.974	1.988
Fo%	74.0	74.2	74.1	72.8	73.8	64.8

n = no. of analyses.

an important factor in their chemistry. Exsolution of orthopyroxene is generally considered as reasonable evidence of the tholeiitic parentage of the host clinopyroxene (Brown 1967, Wilkinson 1967). The data presented here suggests, however, that some Ca-rich clinopyroxenes derived from undersaturated basalt magmas unable to precipitate Ca-poor pyroxenes have compositions capable of exsolving limited amounts of Ca-poor pyroxene, given sufficient time for annealing under moderate to high temperatures.

OLIVINE

Unlike plagioclases and clinopyroxenes, analysed olivines show little evidence of systematic compositional variations with position in the cumulate sequence. The olivines of the basal and crescumulate zones are chrysolites with Fo (mol.%) between 74.2 and 72.8 (Table 5), more iron-rich than the first olivines to crystallize from many basaltic magmas (Brown 1967). In many layered intrusions, cumulus plagioclase and olivine exhibit related variations such that An (mol. %) $\sim$ Fo (mol.%). In the lower part of the layered series of the Rognsund intrusion this relationship is absent. The constancy of olivine compositions may possibly be due to subsolidus reaction with plagioclase, or to partial oxidation, but could also be a primary feature and reflect a relatively limited change in the magmatic FeO: MgO ratio over the crystallization interval represented by the basal and crescumulate zones (Roeder & Emslie 1970). A cumulate-zone sample which has preserved its primary olivine contains Fo_{65} (Table 5), suggesting that a cryptic variation was present in this part of the intrusion.

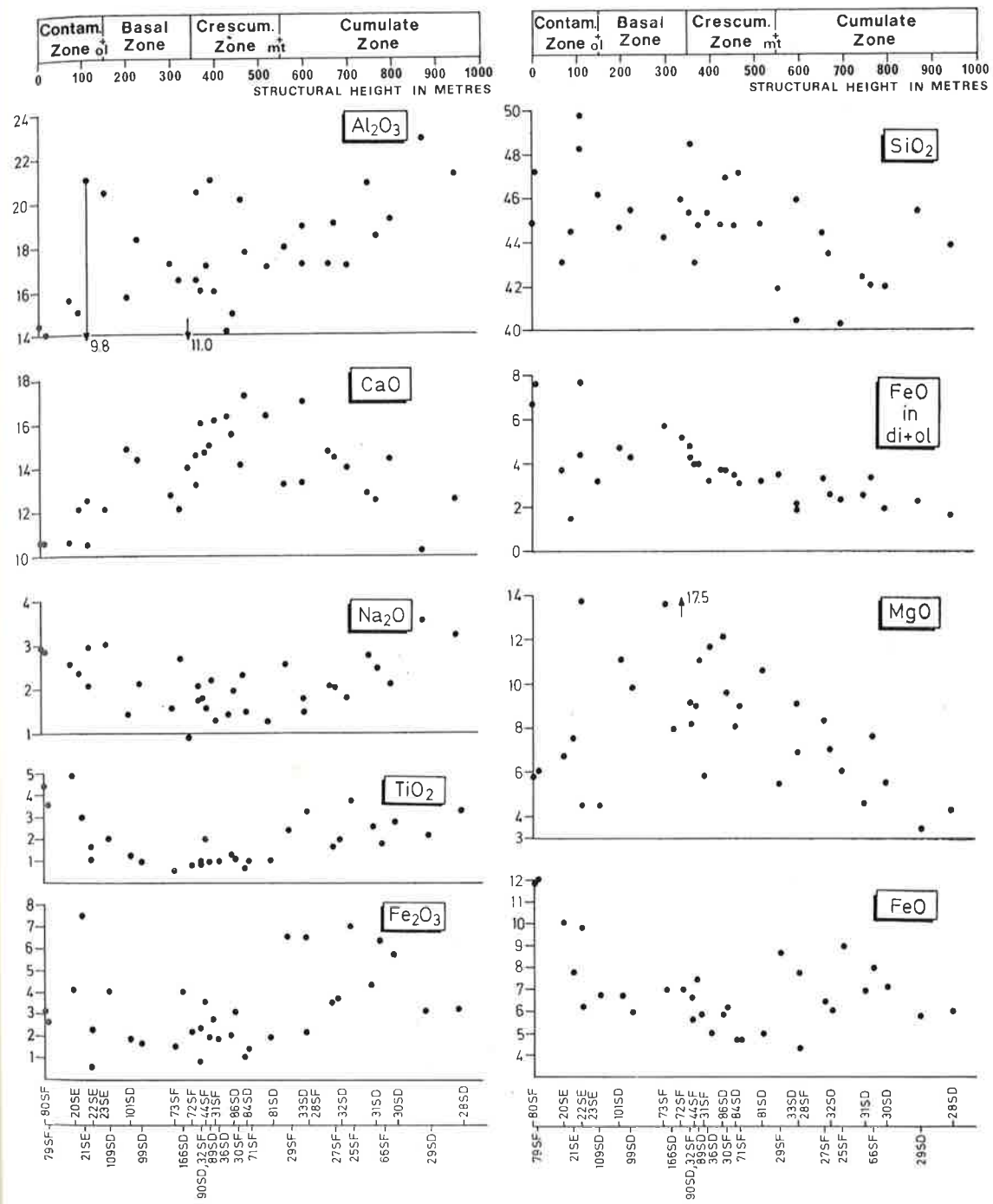

Fig. 23. Major-element compositions of analysed samples plotted against stratigraphic position in the Rognsund intrusion.

Table 6. Major-element analyses of samples from the Rognsund intrusion

Table 6. Major-element analyses of samples from the Rognsund intrusion

Sample no.	80SF	79SF	20SE	21SE	22SE	23SE	109SD	101SD	99SD	73SF	166SD*	72SF	90SD	32SF	44SF	89SD
Strat.pos.	0m	6m	75m	90m	110m	110m	150m	200m	225m	300m	325m	340m	360m	360m	370m	380m
SiO_2	44.92	47.25	43.10	44.50	48.30	49.80	46.20	44.70	45.51	44.25	40.50	46.00	45.44	48.54	43.10	44.85
TiO_2	4.30	3.60	4.95	3.00	1.70	1.10	2.05	1.29	1.03	0.60	4.92	0.85	1.06	0.90	2.05	1.02
Al_2O_3	14.20	14.00	15.50	15.00	21.00	9.00	20.40	15.76	18.29	17.20	16.50	11.00	20.45	16.50	16.00	17.01
Fe_2O_3	3.10	2.62	4.05	7.46	0.60	2.35	4.04	1.89	1.66	1.57	4.05	2.22	0.85	2.40	3.63	2.00
FeO	11.86	12.00	10.05	7.59	6.22	9.83	6.76	6.75	6.00	7.01	9.98	7.01	5.63	6.65	7.45	5.87
MnO	0.20	0.21	0.17	0.18	0.13	0.23	0.15	0.14	0.11	0.13	0.15	0.14	0.10	0.12	0.14	0.12
MgO	5.93	6.00	6.68	7.50	4.50	13.78	4.50	11.10	9.82	13.60	7.93	17.50	8.16	9.18	9.00	11.05
CaO	10.60	10.60	10.60	12.10	12.50	10.50	12.10	14.81	14.35	12.75	12.01	14.00	14.58	13.20	16.00	14.68
Na_2O	2.93	2.83	2.54	2.34	2.93	2.08	3.02	1.42	2.10	1.53	2.67	0.91	1.72	2.05	1.79	1.53
K_2O	0.92	0.27	0.70	0.40	0.53	0.20	0.33	0.25	0.22	0.07	0.33	0.04	0.48	0.14	0.14	0.22
P_2O_5	0.28	0.13	0.23	0.20	0.23	0.23	0.06	0.16	0.04	0.07	0.06	0.06	0.02	0.06	0.05	0.04
H_2O+	0.53	0.39	0.78	0.36	0.68	0.39	0.48	n.d.	n.d.	0.94	0.50	1.15	n.d.	0.15	0.09	n.d.
H_2O-	0.08	0.20	0.19	0.11	0.08	0.16	0.16	n.d.	n.d.	0.07	0.20	0.16	n.d.	0.10	0.86	n.d.
TOTAL	99.85	100.10	99.54	100.74	99.40	100.45	100.25	98.27	99.13	99.79	99.76	101.04	98.49	100.04	100.30	98.36
CIPW norms																
or	5.4	1.6	4.1	2.4	3.1	1.2	1.9	1.5	1.3	0.4	1.9	0.2	2.8	0.8	0.8	1.3
ab	20.8	23.9	20.1	19.8	24.3	17.6	23.2	7.3	9.0	8.2	8.5	7.7	0.6	17.4	2.7	7.3
an	22.9	24.7	28.8	29.2	42.6	16.8	41.1	35.9	39.8	39.9	32.1	25.8	46.7	35.4	35.2	38.9
ne	2.2	-	0.8	-	0.3	-	1.3	2.6	4.7	2.6	7.6	-	3.2	-	6.7	3.0
di	22.9	22.3	17.9	23.3	14.7	17.2	15.0	29.3	24.9	18.4	21.8	34.4	20.6	23.9	35.1	26.9
hy	-	9.8	-	3.0	-	18.4	-	-	-	-	-	0.3	-	8.2	-	-
ol	11.7	6.2	11.0	5.5	9.0	12.6	7.2	16.2	14.8	25.8	11.8	26.3	13.3	8.8	9.4	16.0
mt	4.5	3.8	5.9	10.8	0.9	3.4	5.9	2.7	2.4	2.3	5.9	3.2	1.2	3.5	5.3	2.9
il	8.2	6.8	9.4	5.7	3.2	2.1	3.9	2.4	1.9	1.1	9.3	1.6	2.0	1.7	3.9	1.9
ap	0.6	0.3	0.5	0.5	0.5	0.5	0.1	0.4	0.09	0.2	0.1	0.1	0.05	0.1	0.1	0.09

n.d. = not determined

* Amphibole-plagioclase pegmatite vein

31SF	36SD	86SD	30SF	84SD	71SF	81SD	29SF	33SD	28SF	27SF	32SD	25SF	31SD	66SF	30SD	29SD	28SD
390m	400m	430m	440m	460m	470m	520m	560m	600m	600m	660m	675m	700m	750m	770m	800m	875m	950m
45.20	45.39	44.87	47.00	44.80	47.20	44.90	41.94	40.47	46.00	44.46	43.53	40.29	42.46	42.10	42.03	45.49	43.91
1.50	1.07	1.36	1.15	0.75	1.05	1.07	2.45	3.32	1.05	1.65	2.01	3.80	2.69	1.80	2.83	2.20	3.34
21.00	16.03	14.01	15.00	20.10	17.70	17.08	18.00	18.94	17.20	17.20	19.08	17.20	20.94	18.50	19.32	22.87	21.38
2.81	1.97	2.10	3.13	1.11	1.43	1.95	6.59	6.49	2.25	3.49	3.71	6.97	4.36	6.32	5.74	3.11	3.23
4.99	5.03	5.88	6.22	4.75	4.74	5.00	8.64	7.77	4.27	6.43	6.03	8.93	6.94	7.95	7.11	5.68	6.02
0.10	0.10	0.12	0.13	0.11	0.10	0.10	0.22	0.12	0.10	0.12	0.10	0.18	0.13	0.13	0.11	0.18	0.09
5.80	11.65	12.13	9.60	8.08	9.00	10.60	5.43	6.87	9.10	8.35	7.04	6.00	4.61	7.30	5.50	3.40	4.30
15.00	16.15	16.39	15.50	14.13	17.25	16.31	13.20	13.36	17.00	14.75	14.48	14.00	12.86	12.50	14.38	10.23	12.58
2.21	1.25	1.40	1.95	2.30	1.46	1.25	2.53	1.75	1.46	2.08	2.02	1.79	2.75	2.44	2.10	3.56	3.21
0.14	0.07	0.06	0.17	0.64	0.17	0.08	0.50	0.20	0.14	0.13	0.12	0.14	0.61	0.20	0.13	1.63	0.20
0.10	0.03	0.03	0.08	0.03	0.04	0.03	0.03	0.04	0.05	0.09	0.03	0.06	0.07	0.09	0.05	0.04	0.03
0.60	n.d.	n.d.	0.50	n.d.	0.50	n.d.	0.31	n.d.	0.82	0.85	n.d.	0.54	n.d.	0.63	n.d.	n.d.	n.d.
0.06	n.d.	n.d.	0.09	n.d.	0.03	n.d.	0.19	n.d.	0.04	0.99	n.d.	0.09	n.d.	0.16	n.d.	n.d.	n.d.
99.51	98.74	98.35	100.52	96.80	100.67	98.37	100.03	99.33	99.48	100.59	98.15	99.99	98.33	100.12	99.30	98.39	98.29
0.8	0.4	0.4	1.0	3.8	1.0	0.5	2.9	1.2	0.8	0.8	0.7	0.8	3.6	1.2	0.8	9.6	1.2
13.2	5.8	3.4	12.3	6.7	7.8	5.1	9.7	9.4	7.3	10.3	10.9	9.2	10.9	12.1	10.6	17.3	17.9
46.0	37.9	31.8	31.7	42.6	41.2	40.8	36.3	43.2	40.0	37.2	42.6	38.5	43.0	38.9	42.9	41.6	43.3
3.0	2.6	4.6	2.3	6.9	2.5	2.9	6.3	2.9	2.8	4.0	3.4	3.2	6.6	4.6	3.9	6.9	5.0
21.4	33.3	39.3	35.7	21.9	35.2	31.8	23.5	18.1	34.9	28.3	23.1	24.5	16.4	18.1	22.4	7.2	15.1
-	-	-	-	-	-	-	-	-	-	-	-	-	-	-	-	-	-
6.3	13.7	13.3	10.1	11.8	8.3	12.4	6.5	8.7	7.5	9.8	8.1	5.7	6.2	11.6	4.9	6.9	4.7
4.1	2.8	3.1	4.5	1.6	2.1	2.8	9.6	9.4	3.3	5.1	5.4	10.1	6.3	9.2	8.3	4.5	4.7
2.9	2.0	2.6	2.2	1.4	2.0	2.0	4.6	6.3	2.0	3.1	3.8	7.2	4.9	3.4	5.4	4.2	6.3
0.2	0.07	0.07	0.2	0.07	0.09	0.1	0.07	0.09	0.1	0.2	0.07	0.1	0.2	0.2	0.1	0.1	0.07

Geochemistry

The major- and trace-element petrochemistry of the Rognsund intrusion has been investigated by analysis of 34 *average cumulates* collected at localities plotted in Plate 1. Plots of particular elements or oxides relative to stratigraphic position show high degrees of scatter, but the major trends in the bulk composition of the fractionation products can still be discerned, in particular in the stratigraphic section above the 250 m level. Because of insufficient exposure the lowest part of the basal zone is represented by relatively few analyses.

MAJOR ELEMENTS

Layered series. Analytical results are reported in Table 6, plotted as oxides in Fig. 23 and as normative minerals in Fig. 24. SiO_2 shows highly irregular concentrations, the lowest values being characteristic of the cumulate zone. SiO_2 variation is generally the inverse of the patterns represented by Fe_2O_3, FeO and TiO_2, which vary sympathetically. The negative correlation which exists between SiO_2 and Fe_2O_3 and FeO illustrated in Fig. 26, is largely a product of the variable amounts of cumulus oxides in the cumulate zone. The appearance of cumulus oxides is particularly well marked by TiO_2 concentrations. In the basal and crescumulate zones, TiO_2 maintains a fairly constant level of just under 1 wt.%, corresponding to its concentration in clinopyroxene and the

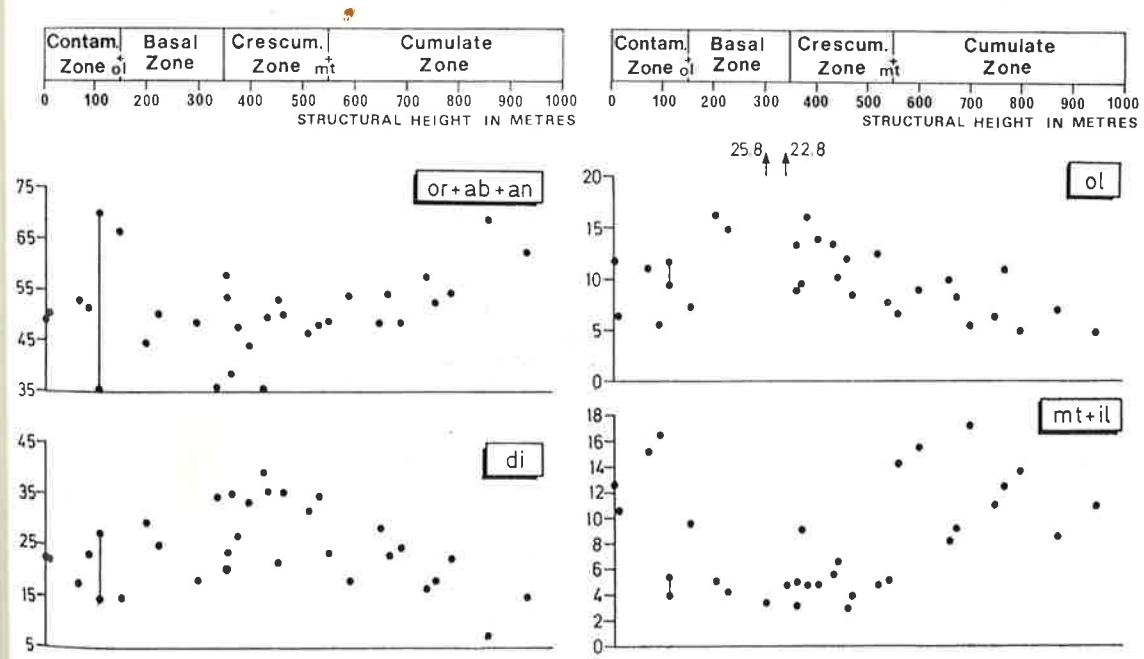

Fig. 24. Normative mineralogy of analysed samples from the Rognsund intrusion.

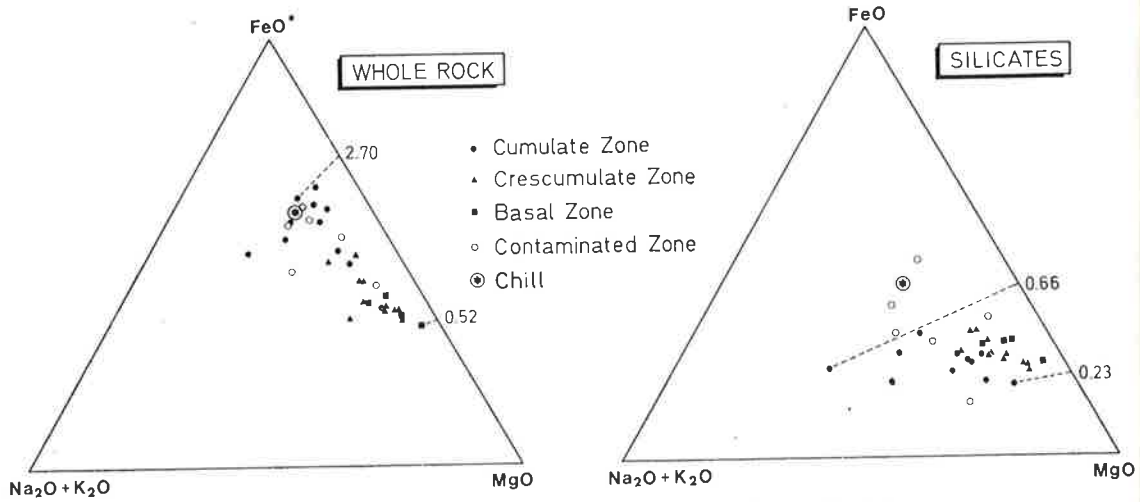

Fig. 25. F.M.A. plot for analysed samples from the Rognsund intrusion ('Whole Rock'), and a plot in which the FeO is that in normative mafics ('Silicates'). The numbers are FeO/MgO ratios.

contribution of intercumulus oxides. At the crescumulate/cumulate zone boundary, TiO_2 rises abruptly and within the cumulate zone never falls below 1.5 wt.% and averages about 2.5 wt.%. Fe_2O_3 variation can be described in the same manner, though concentrations are generally more irregular in the lower part of the layered series and the increase across the lower boundary of the cumulate zone is larger. The appearance of cumulus oxides is displayed in the normative mineralogy by a sudden increase in mt+il at the base of the cumulate zone (Fig. 24). Normative magnetite and ilmenite are fairly constant in the basal and crescumulate zones but vary considerably above the phase boundary due to the varying amounts of cumulus oxides in the sampled cumulates.

FeO variation is somewhat different from that of TiO_2 and Fe_2O_3 in the two lowermost zones. While TiO_2 and Fe_2O_3 appear to be fairly constant, FeO decreases from about 7% to under 5%. This behaviour must be attributed to compositional variations in the cumulus olivine and pyroxene and/or a fall in the mode of either or both phases. Plotting FeO minus FeO combined in normative magnetite and ilmenite produces a progressively falling curve for FeO concentration associated with normative silicates with height, throughout the layered series (Fig. 23). MgO is highly scattered but appears to show a more rapid decrease than FeO with stratigraphic height, suggesting that both MgO and FeO variations are the result of a decrease in the amount of cumulus Mg–Fe silicates upwards in the layered sequence, combined with a change in their compositions towards more iron-rich solid solutions. A decrease in normative mafics is clear in Fig. 24, the fall being compensated by increases first in oxides and later in plagioclase.

In the F-M-A triangle, the analyses define an iron-enrichment trend, due largely to the effect of cumulus oxides in increasing the $FeO^t + MnO/MgO$ ratio

Fig. 26. Plot of the sum of iron oxides against SiO_2 for cumulates and contaminated-zone rocks. Symbols as in Fig. 25.

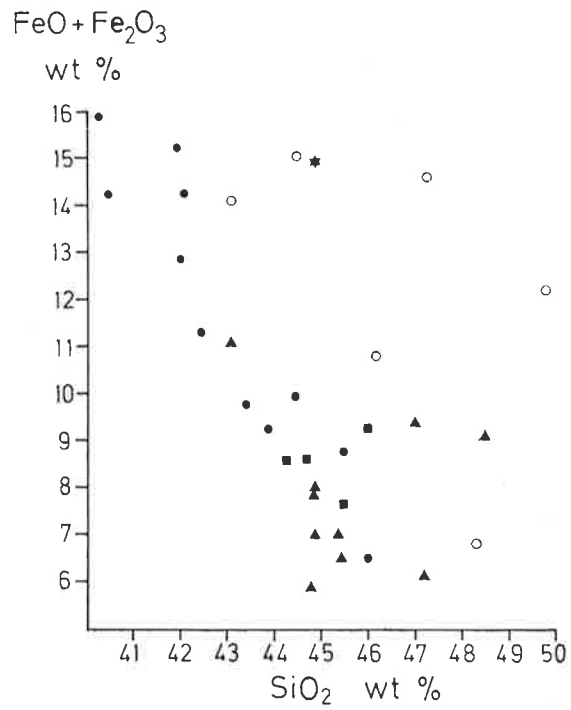

(Fig. 25). Subtracting from FeO^t an amount corresponding to iron oxides combined in normative mt+il changes the trend to one of alkali enrichment, the FeO^t/MgO ratio varying only from 0.23 to 0.66 and without any relationship to the stratigraphic position of the analysed samples. The alkali enrichment trend corresponds to the upward decrease in the normative mafic minerals and the increase in plagioclase. These relationships suggest that it is unlikely that the parent magma underwent any significant degree of iron-enrichment during the fractionation interval represented by the visible crystallization products.

CaO and normative diopside have similar patterns of variation (Figs. 23, 24). Both seem to first increase, reach a maximum in the crescumulate zone, and then fall throughout the cumulate zone. Plots of Al_2O_3, Na_2O and normative feldspar components are also essentially identical. They all show an increase towards the summit of the visible part of the cumulate zone.

Contaminated zone rocks are little different in the principal normative minerals from those of the cumulate zone (Fig. 24), and many of the major elements occupy ranges similar to those of the cumulates. CaO is generally lower, however, than in the cumulate rocks and some samples have higher SiO_2. In a $FeO + Fe_2O_3/SiO_2$ plot (Fig. 26), the contaminated zone rocks are well separated from the cumulates. The former are generally richer in SiO_2, than the cumulates for particular concentrations of iron oxides. In some cases, this

Table 7. Trace-element analyses of samples from the Rognsund intrusion

Sample no.	80SF	79SF	20SE	21SE	22SE	23SE	109SD	101SD	99SD
Strat.pos.	0 m	6 m	75 m	90 m	110 m	110 m	150 m	200 m	225 m
Ni ppm	407	380	334	389	392	893	419	551	482
Cu	19	39	35	50	19	104	24	55	13
Zn	89	94	71	79	64	102	74	58	52
Rb	31	5	28	8	9	3	5	7	7
Sr	481	416	633	508	710	308	748	460	624
Y	16	13	8	9	8	13	12	5	5
Zr	56	51	45	48	67	46	54	21	15
Nb	31	16	17	13	19	17	22	2	4
La	25	10	14	12	12	14	15	2	3
Ce	45	34	28	29	34	41	30	10	11
Nd	32	24	19	18	19	27	25	6	4

Sample no.	31SF	36SD	86SD	30SF	84SD	71SF	81SD	29SF	33SD
Strat.pos.	390 m	400 m	430 m	440 m	460 m	470 m	520 m	560 m	600 m
Ni ppm	571	618	688	512	534	765	644	384	353
Cu	37	95	81	54	31	120	96	36	36
Zn	45	43	45	48	47	58	44	79	66
Rb	4	4	2	7	21	1	2	9	7
Sr	708	408	453	508	639	719	481	807	630
Y	3	5	6	4	6	3	5	6	2
Zr	9	26	29	18	10	5	20	59	8
Nb	n.d.	1	2	1	5	n.d.	n.d.	33	n.d.
La	5	n.d.	n.d.	2	8	n.d.	n.d.	16	n.d.
Ce	12	10	11	14	14	9	9	26	12
Nd	5	5	5	7	7	1	4	15	5

n.d. = not detected.

results in normative opx, while the cumulates are almost invariably ne-normative (Table 6).

The two samples collected closest to the gabbro/aureole contact are chemically rather similar to the marginal chill, while further from the contact, the appearance of cumulus minerals causes irregular fluctuations in composition (compare samples 22 & 23 SE from the same locality).

The chill (80 SF), collected within a metre of the contact, is basaltic in character, differing only in lower SiO_2 and Al_2O_3 and higher total FeO and TiO_2 from an average of 1996 basalts (Manson 1967). It is highly significant that ne is present in the CIPW norm of the chill, despite the general chemical similarity of the chill with other analysed samples from the contaminated zone (Figs. 23, 27) and the possibility of assimilation of the adjacent metasediments. Arguments based on trace-element values suggest that assimilation was much less than 10–15 wt.% (see below). Incorporation of this amount of material of composition similar to the mean composition of the psammites and neosomes reported in Table 1 would not change the chemical character of the chilled margin of the Rognsund gabbro to any significant degree.

Table 7 continued

Sample no.	73SF	166SD*	72SF	90SD	32SF	44SF	89SD
Strat.pos.	300 m	325 m	340 m	360 m	360 m	370 m	380 m
Ni ppm	596	245	733	620	741	553	594
Cu	58	24	21	19	255	39	35
Zn	38	71	56	47	54	58	54
Rb	8	3	3	16	4	4	5
Sr	563	822	338	713	470	522	512
Y	4	8	3	4	4	5	4
Zr	29	24	18	5	14	24	17
Nb	9	12	1	n.d.	2	2	n.d.
La	3	5	3	3	2	3	2
Ce	11	21	7	11	12	12	11
Nd	5	16	2	6	6	7	6

Sample no.	28SF	27SF	32SD	25SF	31SD	66SF	30SD	29SD	28SD
Strat.pos.	600 m	660 m	675 m	700 m	750 m	770 m	800 m	875 m	950 m
Ni ppm	497	473	475	452	425	417	341	517	408
Cu	30	22	25	40	62	50	15	30	36
Zn	35	57	55	75	66	67	58	72	53
Rb	4	2	2	5	16	6	2	48	4
Sr	572	626	632	743	885	697	696	1085	929
Y	5	4	3	3	3	2	4	4	2
Zr	22	12	6	9	15	9	6	n.d.	n.d.
Nb	1	n.d.	n.d.	n.d.	n.d.	n.d.	n.d.	n.d.	n.d.
La	4	4	3	3	4	4	2	1	5
Ce	11	13	15	10	16	13	14	11	11
Nd	6	5	7	4	7	6	7	4	6

* Amphibole–plagioclase pegmatite vein.

TRACE ELEMENTS

Layered series. Of the analysed trace elements, Sr and Ni have the highest concentrations (Table 7). Sr correlates with Na_2O, Al_2O_3 and normative or+ab+an (compare Fig. 27 with Figs. 23 & 24), and Ni correlates weakly with normative ol.

Both Cu and Zn maintain fairly constant concentrations throughout the layered series (Fig. 27), as do Rb, Y, Zr, Nb and the light REE, at lower levels of concentration. Nb concentrations, as well as those for La and many of the Y values, lie close to, or below, the limits of sensitivity for the analytical methods employed (described in Robins & Takla 1979). One cumulate (29SF), however, is anomalous in that significant REE, Y and Nb are present. Chondrite-normalized values for this sample give a light-element enriched REE distribution pattern (Fig. 28). If the concentrations of the incompatible elements in this cumulate are characteristic of an intercumulus assemblage, then none of the other sampled cumulates have the trace-element behaviour to be expected in orthocumulates.

Contaminated zone rocks have trace-element compositions rather different from those of the cumulates, particularly with respect to Zr, Nb, REE and Y. Ni, Cu,

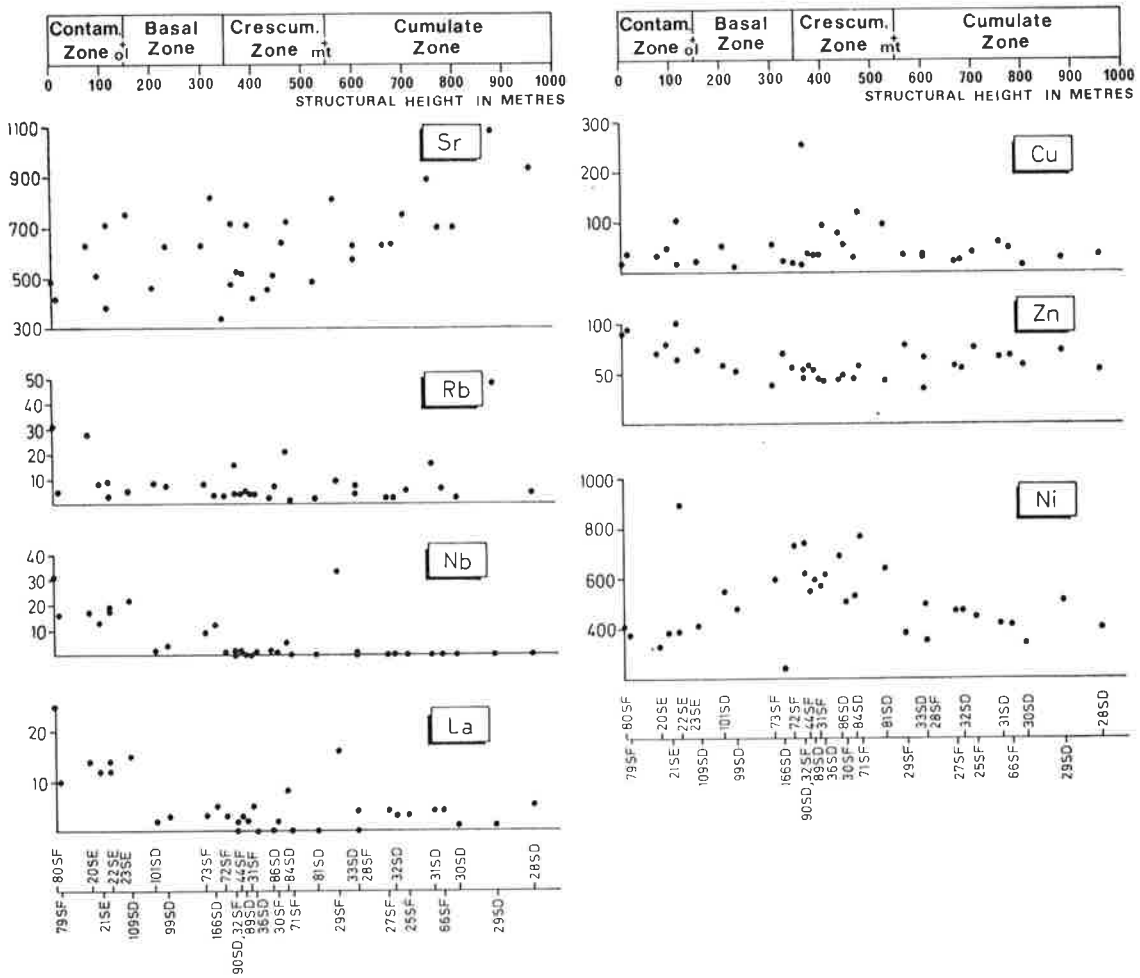

Fig. 27. Trace-element compositions of analysed samples plotted against stratigraphic position in the Rognsund intrusion.

Rb and Sr do not differ significantly in the contaminated zone from the equivalent concentrations in parts of the layered series. Zn is, however, very slightly higher than in the cumulates, and Ni is lower than in the overlying zones (Fig. 27).

Zr & Nb concentrations in the contaminated zone are above 45 and 16 ppm respectively. Mean values for Zr and Nb are respectively 3.3 and 6.9 times higher in the contaminated-zone samples than in the cumulates (Table 8). In terms of chondrite-normalized distributions, plotting Y instead of a heavy REE, the contaminated-zone rocks are light-element enriched (Fig. 28), with mean abundances 3–5 times higher than the cumulates (Table 8).

The Y/Nb ratios of the contaminated-zone rocks (and the chill) fall in the range typical of continental and ocean-island alkaline basalts (Pearce & Cann

Table 8. Mean residual trace-element compositions of anatexites (and psammites), contaminated zone rocks and layered series cumulates

	Anatexites		Contamin. zone		Cumulates	
	14		7		27	
	$\bar{X}$	S	$\bar{X}$	S	$\bar{X}$	S
Y	42.0	9.7	11.3	3.0	4.1	1.4
Zr	436.4	111.3	52.4	7.6	15.9	12.0
Nb	24.6	6.7	19.3	5.9	2.8	6.7
La	48.6	10.7	14.6	4.9	3.2	3.2
Ce	86.4	15.8	34.4	6.4	12.5	3.8
Nd	46.7	10.3	23.4	5.1	6.1	3.1
Chondrite – normalized						
La	162.0		48.7		10.7	
Ce	102.9		41.0		14.9	
Nd	80.5		40.3		10.5	
Y	23.3		6.3		2.3	
La/Y	6.9		7.7		4.7	

$\bar{X}$ = arithmetic average.
S = standard deviation.
n = no. of analyses.

Table 9. Results of subtraction calculations for residual trace-element composition of chill

	Chill	Chill – wt% Anatexites			Anatexites
	80SF	5%	10%	15%	$\bar{X}$
Y	16	15	13	11	42
Zr	56	36	14	–11	436
Nb	31	31	32	32	25
La	25	24	22	21	49
Ce	45	43	40	38	86
Nd	32	31	30	29	47

$\bar{X}$ = arithmetic average.

1973), while in the metasediments and neosomes of the contact metamorphic aureole Y/Nb ratios are generally > 1 (Table 1).

Apart from high Ni, low Cu, Rb, Y and Zr the mean trace-element composition of the analysed contaminated-zone rocks is rather similar to that of average basalts, suggesting that assimilation of metasedimentary xenoliths was limited in degree.

The chill. Comparing the mean compositions of the contaminated-zone rocks, and the metasediments and neosomes from the contact metamorphic aureole (Table 1), one of the most striking differences lies in Zr concentrations. The felsic contain in excess of 8 times more of this element than the mafic (Table 8). Subtraction calculations show that Zr in the chill goes to zero at between 10 and 15% assimilated material having a composition equal to the mean of Table 1 (Table 9). This simple calculation suggests that the trace-element com-

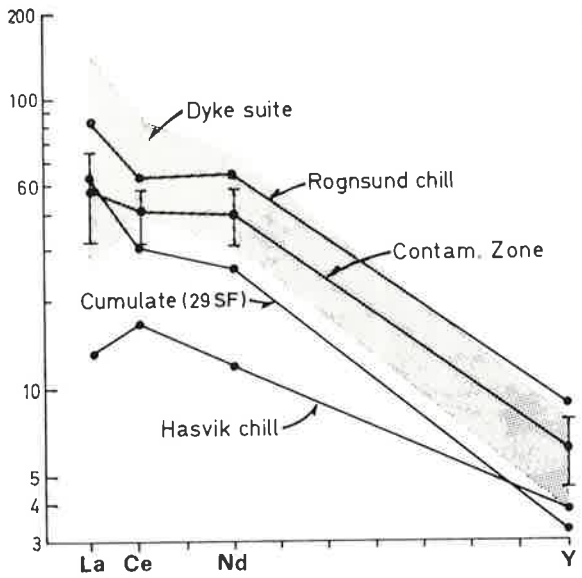

Fig. 28. Chondrite-normalized REE distribution patterns for various samples from the Rognsund intrusion. Y is plotted in place of Ho. Normalizing factor is a mean of 20 chondrites (Haskin et al. 1966). Shaded area is the field occupied by an alkali olivine basalt dyke suite emplaced subsequently to the Rognsund intrusion (Robins & Takla 1979). Vertical bars are 2 standard deviations long.

Table 10. Comparison of the Rognsund chill with the Hasvik gabbro chill, and post-Rognsund intrusion dykes (n = 23)

	Rognsund chill		Hasvik chill	Dykes	
	80SF	80SF – 5wt.% il	P338	$\bar{X}$	D21
SiO_2	45.26	47.64	50.09	45.44	48.92
TiO_2	4.33	1.76	1.03	1.85	1.93
Al_2O_3	14.31	15.06	15.71	13.23	15.55
Fe_2O_3	3.12	3.28	0.80	3.00	1.94
FeO	11.95	10.08	7.22	8.74	9.07
MnO	0.20	0.21	0.14	0.17	0.14
MgO	5.98	6.29	9.47	13.15	7.09
CaO	10.68	11.24	13.00	11.00	11.19
Na_2O	2.95	3.11	2.12	2.41	3.19
K_2O	0.93	0.98	0.27	0.78	0.73
P_2O_5	0.28	0.29	0.14	0.25	0.24
	100.00*	100.00*	100.00*	100.00*	100.00*
FeO†	14.76	13.03	7.94	11.44	10.82
Ni	410	432	558	450	213
Cu	19	20	12	24	14
Zn	90	95	64	86	81
Rb	31	33	4	17	10
Sr	485	511	386	368	450
Y	16	17	7	11	10
Zr	56	59	39	79	69
Nb	31	33	10	20	15
La	25	26	4	20	21
Ce	45	47	14	48	46
Nd	32	34	7	28	24

* Recalculated to 100%, water-free.
$\bar{X}$ = arithmetic average.

position of this chill may be closely similar to that of an uncontaminated magma.

Comparing trace-elements in the chill with those determined in the olivine–tholeiitic marginal chill of the Hasvik gabbro (Robins & Takla 1979) reveals that the former is enriched in all of the analysed incompatible elements (Rb, Sr, Y, Zr, Nb, La, Ce and Nd) relative to the latter, and depleted in Ni (Table 10 and Fig. 28). Good agreement exists, however, between the trace-element composition of the chill and the mean of 23 amphibolite dykes of alkali olivine basalt affinities from the Seiland province (Robins & Takla 1979), exceptions being higher Rb and Y in the former (Table 10).

Petrogenesis

EVALUATION OF THE CHILL

Recent studies (e.g. McBirney 1975) suggest that chilled margins to layered intrusions may be unreliable as evidence of the composition of initial magmas, due to assimilation of wall rocks and deuteric effects. Other phenomena, such as flow differentiation, temporal variations in the compositions of the intruding magma, and slumping of marginal border groups and contact of liquids at various stages of fractionation with the walls, may also contribute to a chilled zone being unrepresentative of an initial magma composition (Robins & Gardner 1974, Carmichael, Turner & Verhoogen 1974). Arguments presented above suggest that the analysed chill from the Rognsund gabbro could not have been significantly contaminated by assimilation of the psammitic wall rocks. Its composition is, however, such that it is questionable whether it could represent the parental magma.

Unless Ti-bearing oxides are under-represented in the sampled cumulates from the cumulate zone, 4.3% TiO_2 in the chill appears to be excessively high. In samples from the upper part of the basal zone and from the crescumulate zone, TiO_2 has a fairly constant level ($\bar{x}$ = 1.1 wt.%, s = 0.37) attributed to its concentration in cumulus clinopyroxene and the intercumulus material. Correcting for clinopyroxene crystals with an average of 1.1% TiO_2 (from Table 3) and a mean normative bulk of 29% (from Table 6) gives 0.66% as a very rough estimate of intercumulus TiO_2. Accepting the hypothesis that the samples were orthocumulates, and that the mode of primocrysts in such rocks cannot exceed about 60% (Wager & Brown 1968), the content of TiO_2 in the parent to these cumulates is likely to have been in the region of 1.6–2.2 wt.%. This is rather higher than the estimate of between 0.9 and 1.2% TiO_2 required for the co-precipitation of magnetite and ilmenite from basaltic liquids (Carmichael, Turner & Verhoogen 1974).

FeO in the chill is also much higher than in the basal- and crescumulate-zone cumulates, even though these show a quite distinct upward trend towards lower concentrations of Fe^{2+}. The upward decrease in FeO in these cumulates can be ascribed to fractionation of a magma containing a maximum of about

10 wt.% FeO. Al_2O_3 in the chill is notably low at 14.2 wt.% compared to the concentration of this oxide in the layered series cumulates. In the latter, Al_2O_3 rarely falls below 16%, and there is some evidence that it increases in the upper part of the cumulate zone.

The oxides discussed above are those, together with SiO_2 in which the chill differs considerably from average basaltic abundances. It would appear that the chill is depleted in Al_2O_3, and possibly SiO_2, and enriched in FeO and TiO_2 relative to the probable parent to the Rognsund intrusion. These distinctive chemical features are also shared by the non-cumulate part of the contaminated zone, and they may be attributed to the early emplacement of a relatively evolved basalt in which an Fe-Ti oxide was a liquidus phase. The chill and the contaminated zone may have become enriched in oxides by pre-emplacement differentiation of this magma or by rapid gravitational accumulation immediately after its intrusion. The mineralogy of the cumulate zone shows that magmas capable of precipitating ilmenite and magnetite existed in the Rognsund intrusion at an early stage of differentiation. Ilmenite was also a liquidus phase in the Skærgaard magma during the crystallization of LZa (Hoover 1978). Subtraction of as little as 5 wt.% of pure ilmenite from the analysis of the Rognsund chill brings its composition into the ranges appropriate to the parent discussed above (Table 10). The intitial emplacement must have been followed by a less evolved basalt forming the main bulk of the intrusion.

COMPARISON OF THE CHILL WITH LATER DYKES

As noted earlier, the Rognsund gabbro is intruded by swarms of metamorphosed basic and ultrabasic dykes (Robins & Takla 1979). The dykes form a suite of sodic alkali olivine basalt affinities with a mode in the alkali picrite compositional range. Blastoporphyritic examples are petrographically similar to the cumulates of the Rognsund intrusion in that they contain diopside and salite with exsolved spinel and ilmenite lamellae (Robins & Takla 1979, Fig. 8). Although emplaced subsequently to the development of the metamorphic fabric in the gabbro, the dykes are ascribed particular importance in clarifying the nature of the gabbro parent.

Comparing the major-element geochemistry of the chilled margin of the Rognsund gabbro with the ranges established for the later dykes from 44 analyses, reveals that for the majority of the oxides there is co-incidence. The concentrations of TiO_2 and FeO in the chill lie, however, well above the upper limits of the variation shown by the dykes. Total iron as FeO in the dykes maintains a fairly constant level throughout the suite, averaging 11.31 wt.% ($s = 0.58$), while TiO_2 is more variable but never exceeds 2.6%. The chill also has an MgO concentration lying 1 wt.% beneath the lowest value recorded from the dykes.

Apart from slightly high Y, the trace-element composition of the chill falls well within the ranges expressed by the dyke suite. Both seem to be typified by light-element enriched chondrite-normalized REE patterns (Fig. 28), quite distinct in terms of absolute enrichment from the chilled olivine tholeiite from

the Hasvik layered intrusion on the adjacent island of Sørøy (Robins & Takla 1979).

The analysed dyke containing least MgO is similar to the Rognsund chill in all major elements except for higher SiO_2 and Al_2O_3 and lower TiO_2 and FeO^t (Table 10). The dyke contains 1.2% ne and can be classified as an alkali olivine basalt. Moreover the major-element composition of the dyke fulfils the specifications for a parent magma required by the trends expressed by the layered series cumulates, i.e. TiO_2 lies between 1.6 and 2.2 wt.%, FeO is less than 10 wt.% and Al_2O_3 exceeds 15 wt.%. Fairly good agreement also exists between the alkali olivine basalt dyke and the composition of the chill corrected for 5 wt.% il (Table 10), except for Fe_2O_3 and MnO which are higher in the chill. The latter oxides could also have been incorporated in a Fe-Ti oxide phase but have not been corrected for by the simple calculation employed.

In terms of trace elements, the alkali olivine basalt dyke is poorer in Ni, Rb Y, Nb and Nd than the chill to the Rognsund gabbro, but general agreement exists between the other analysed traces (Table 10).

The author suggests that both the analysed alkali olivine basalt dyke-rock intruded into the Rognsund gabbro, and the chill corrected for about 5 wt.% il, may be approximate models for the major-element composition of the parent magma to the Rognsund intrusion.

EVALUATION OF THE CUMULUS PARAGENESIS

In the absence of cumulus and intercumulus Ca-poor pyroxene, one of the most sensitive indicators of the nature of the parent to the Rognsund intrusion is the composition of the cumulus clinopyroxenes. As discussed earlier, the latter are diopsides and salites rich in Al_2O_3. Compared with the early clinopyroxenes from tholeiitic layered complexes, the Rognsund pyroxenes are abnormally Ca-rich, and are similar to the low-pressure pyroxenes found in alkali olivine basalt minor intrusions, except for their moderate TiO_2 contents. In the basal and crescumulate zones, TiO_2 increases with Fe-enrichment of the pyroxene, but any further rise in Ti is curtailed by the early crystallization of Fe-Ti oxides. The same type of pattern as for TiO_2 distribution in pyroxene in the Rognsund gabbro is more clearly displayed by Al_2O_3, and is ascribed to the same cause. That the cumulus magnetite was Al-rich is clearly indicated by its high degree of lamellar and granular spinel exsolution. It has been shown that the clinopyroxenes have a small excess of Al^4 relative to that required for titanpyroxene and Ca-Tschermaks molecules, and that this is probably mainly balanced by Cr^{+3}. The characteristic exsolution of picotite also suggest that the clinopyroxenes were chromian varieties. Analyses of two exsolved clinopyroxenes gave a mean of 0.3 wt.% Cr_2O_3, slightly lower than in the endiopsides of the Blue Mountain alkali ultrabasic–gabbro complex, but of the same order as the titanaugites from the same complex (Grapes 1975). While Cr can be expected to be equally high in early clinopyroxenes from both alkaline and tholeiitic magmas (Kuno 1975), the Rognsund gabbro clinopyroxenes are enriched in Na_2O relative to the latter. Data presented for Hawaiian pyroxenes (Fodor &

Keil 1975), suggests that the sodium content of clinopyroxenes may be a useful relative measure of the Na_2O concentrations of their parents. The relatively high concentration of Na_2O in the Rognsund gabbro pyroxenes may by this criterion reflect a parent basalt more alkali-rich than a tholeiite. The pressure under which crystallization took place would, however, tend to increase the equilibrium contents of $NaAlSi_2O_6$ (Kushiro 1969), as well as depress the solubility of $CaTiAl_2O_6$ (Onuma & Yagi 1971) in Ca-rich pyroxenes on the liquidus with plagioclase and olivine. The higher liquidus temperature at these pressures will also enhance the solubility of $CaAl_2SiO_6$ (Thompson 1974). Compared to their low-pressure equivalents, pyroxenes crystallizing from alkali olivine basalts under moderate pressures should be poorer in titanium and richer in aluminium; the Rognsund pyroxenes appear to fulfil these criteria.

Pyroxene phenocrysts from blastoporphyritic amphibolites which postdate the Rognsund gabbro are also diopsides and salites with moderate amounts of TiO_2 and Al_2O_3. Their compositional range, from $Ca_{49.3}Mg_{42.4}Fe_{8.3}$ to $Ca_{47.5}Mg_{39.0}Fe_{13.5}$, is similar to that in the lowest part of the Rognsund cumulate sequence; they co-exist with olivine of $Fo_{73.5}$ to $Fo_{69.4}$. The similarities in the mineral compositions in dykes which have major- and trace-element chemistries typical of alkali picrites and ankaramites (Robins & Takla 1979), and in the cumulus mafic-mineral paragenesis of the Rognsund intrusion strongly suggests that also the latter crystallized from a magma of alkali olivine basalt affinity.

INTERPRETATION OF THE CRYPTIC VARIATION

In this section, the chemical and mineralogical variations of the cumulates are summarized and as far as is possible interpreted in terms of the evolution of the supernatant magma. The nearly linear variation of the Ab-contents of cumulus plagioclases and Fe-contents of cumulus clinopyroxenes with stratigraphic height suggests that over the preserved vertical sequence, stratigraphic height can be correlated with the percentage of the parent magma crystallized. With the data at hand, the latter cannot, however, be quantified.

The initial cumulates consisted of plagioclase ($\sim An_{84}$), clinopyroxene ($\sim Ca_{47}Mg_{45}Fe_8$) and olivine (possibly about Fo_{75}), compatible with the earliest stages of fractionation of an alkali olivine basalt magma. Subsequent fractionation resulted in depletion of the magma in FeO, MgO, CaO and Ni, and an increase in TiO_2, Fe_2O_3, the FeO^t/MgO ratio and probably Na_2O, Al_2O_3 and SiO_2. Elements not entering cumulus phases, such as K and P, also must have increased. As noted above, the composition of the olivine could indicate that changes in the FeO/MgO ratio in the liqiud were relatively slight. Fractionation of clinopyroxene should, however, have led to enrichment of FeO relative to MgO. Falling temperatures, accumulation of alkalies and reduction in magma volume possibly led to progressive oxidation of ferrous iron to ferric (Carmichael, Turner & Verhoogen 1974), offsetting the increase in FeO/MgO. Olivine is the fractionating phase which can determine by its proportion whether a liquid embarks on a course of absolute iron-enrichment, or one of depletion in FeO. In the Rognsund gabbro, the initial cumulates contained

sufficient olivine relative to plagioclase and clinopyroxene that they were enriched in FeO relative to the parent magma.

Fractionation was accompanied by an increase in Al_2O_3 and TiO_2 in clinopyroxene as it became gradually iron-enriched. Iron-enrichment of the fractionating pyroxene was compensated in the cumulates by its diminishing volumetric significance. Crystallization of cumulus magnetite and ilmenite commenced at a certain level of TiO_2 and Fe_2O_3 in the magma, increasing the rate of SiO_2 enrichment. The appearance of ilmenite probably led to subtraction of Ti from the magma during subsequent fractionation. The attainment of five-phase crystallization reduced the content of TiO_2 and Al_2O_3 in clinopyroxene, which at this stage had a composition of approximately $Ca_{48}Mg_{41}Fe_{11}$, and occurred at the expense of the weight fraction of the other mafic minerals in the fractionation products. The oxides–silicates relationships may be a result of the magma attaining a threshold value for silica activity at which the right-hand sides of the followng reactions would be favoured:

$$2CaTiAl_2O_6 + Fe_2SiO_4 + 3SiO_2 = 2FeTiO_3 + 2CaAl_2Si_2O_8$$
$$CaAl_2SiO_6 + SiO_2 = CaAl_2Si_2O_8$$

At the same time, however, silica activity was insufficient to favour the right-hand side of a reaction of the type:

$$MgAl_2O_4 + SiO_2 = MgAl_2O_6$$

Since the abundance of spinel exsolved from the cumulus magnetite shows that the magnetite was an aluminous variety.

Further fractionation was accompanied by continuation of the iron-enrichment in clinopyroxene and sodium-enrichment in plagioclase. The latter mineral appears to have increased in importance in the crystallization products and towards the close of the fractionation history, represented by the upper part of the exposed cumulate stratigraphy, had a composition of around An_{65}. At the stage represented by the uppermost cumulates, depletion of the magma in FeO, MgO and CaO appears to have continued.

Plotting the principal normative minerals of the cumulates within the simplified basalt tetrahedron (Yoder & Tilley 1962) illustrates the dispersed but distinct trend towards plagioclase enrichment with stratigraphic height (Fig. 29). The cumulate trend bears no relationship, however, with the estimated position and shape of the three-phase cotectic in the dry system at 1 kb. Better agreement may be obtained at higher pressures and H_2O fugacities, with the consequent reduction of the plagioclase field and expansion of the field for diopside (Yoder 1965, Presnall et al. 1978). The relationships portrayed in Fig. 29 suggest that in the natural iron-bearing system the cotectic has a distinct concave curvature away from clinopyroxene.

The magmatic trend inferred from the Rognsund intrusion has close similarities with those established for mildly alkaline basalts through analysis of

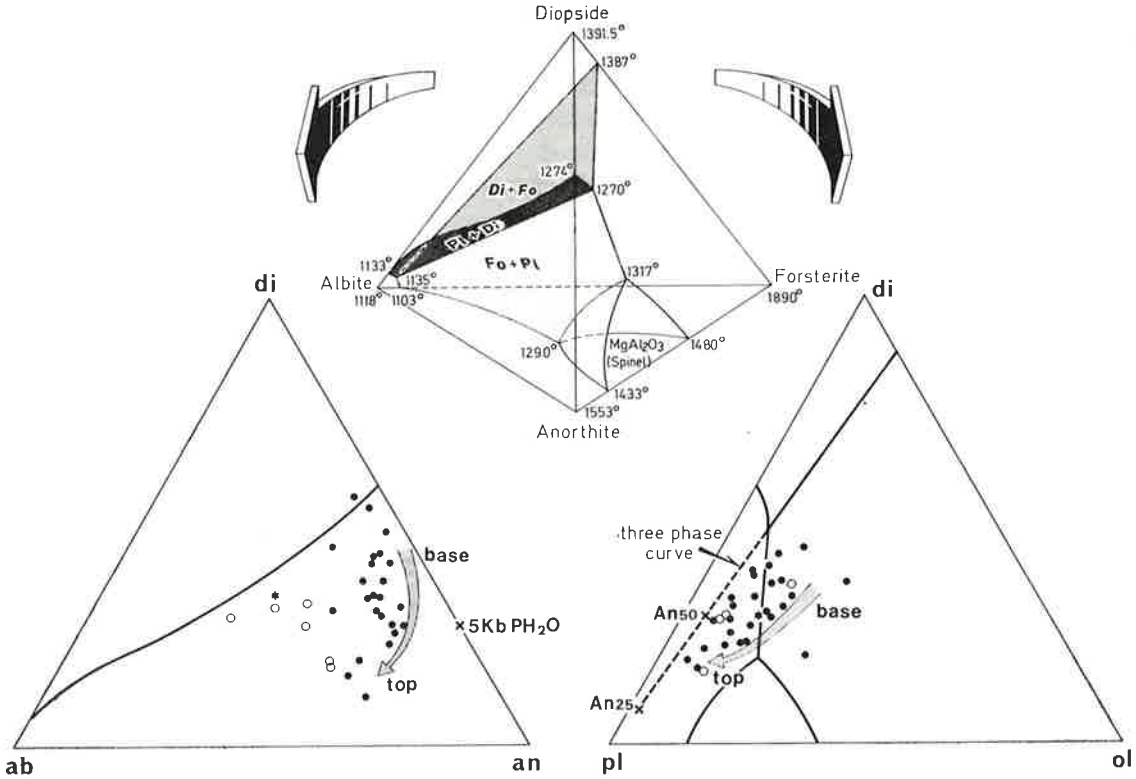

Fig. 29. Rognsund intrusion average cumulates (dots), contaminated-zone rocks (rings) and chill (asterisk) plotted in projections of the simplified basalt tetrahedron (Yoder & Tilley 1962).

volcanic products, and contrasts strongly with the models erected on the basis of studies of layered tholeiitic complexes. The reduction in FeO in the Rognsund gabbro liquid, the more rapid fall in MgO, and the early appearance of Fe-Ti oxides are particularly important in this respect, being similar to that observed in several alkali basalt suites (Williams 1933, MacDonald 1944, Kuno 1968, Baker 1969, Leeman & Rogers 1970), and quite different from the trends characterizing tholeiitic basalts involving high degrees of iron-enrichment. Since a trend of depletion in FeO was apparently established in the Rognsund magma before magnetite and ilmenite crystallization, these different fractionation paths cannot be ascribed to differences in oxygen fugacity alone.

The early fractionation products of Al_2O_3-rich tholeiitic basalts are characterized by a high proportion of plagioclase, as exemplified by the hidden and lower zones of the Skaergaard intrusion (Maaløe 1976), and the lower parts of the Kiplapait (Morse 1969) and Michikamau intrusions (Emslie 1965). Fractionation of plagioclase and clinopyroxene can alone result in iron-enrichment, and for the majority of basalts also to silica depletion. The Rognsund gabbro suggests that the alkali-enrichment fractionation trend followed by alkali olivine basalts may be a function of their moderate Al_2O_3 contents and under-

saturated character, such that olivine is volumetrically more important in the crystallization products than in the case of tholeiitic basalts. Simple calculations show that, depending on the amount of clinopyroxene separating (0–40 wt.%), crystallization of chrysolitic olivine to the extent of 45–35 wt.% of the fractionating minerals (olivine, clinopyroxene and plagioclase) will produce an iron-depletion trend in a basalt initially containing 10 wt.% FeO (see also Roeder & Emslie 1970). In this respect, it is worth noting that in both the alkali olivine basaltic Lilloise and Blue Mountain intrusions olivine-rich cumulates form a major part of the cumulate sequences (Brown 1973, Grapes 1975). Cumulates and intrusive facies dominated by olivine also are very commonly associated with alkali olivine basalt minor intrusions (Tyrell 1917, Drever & Johnston 1967, Philpotts 1974), while in the equivalent tholeiitic intrusions they are relatively rare (Carmichael, Turner & Verhoogen 1974).

The fractionation represented by the Rognsund intrusion differs, however, from many other examples in that all the major silicate phases were on the liquidus of the parent magma, and were joined by oxides after a limited fall in temperature. This suggests that the parent was not a primary alkali olivine basalt liquid but had undergone previous fractionation at pressures not substantially different from those pertaining in the Barrovian metamorphic environment of the Rognsund intrusion.

Acknowledgements. — The author thanks Professors G. M. Brown, S. Maaløe and B. A. Sturt for their critical reviews of an early draft of the manuscript. The figures were drawn by cartographers E. Irgens, J. Lien and M. Adachi, and amanuensis M. Tysseland, S. Trovik, E. Krogh and P. Gardner assisted with the analytical programme. The staff of the X-ray and electron microprobe laboratories of the Departments of Earth Sciences at the Universities of Leeds and Durham are also thanked for their help. The work was supported financially by the Norwegian Research Council for the Sciences and Humanities (N.A.V.F., project D. 48.22–18) and is contribution no. 48 to Project 27 (The Caledonide Orogen) of the International Geological Correlation Programme.

REFERENCES

Baker, I. 1969: Petrology of the volcanic rocks of Saint Helena island, South Atlantic. *Bull. Geol. Soc. Am. 80*, 1283–1310.

Barth, T. F. W. 1927: Die Pegmatitgänge der Kaledonischen Intrusivgesteine im Seiland-Gebiete. *Norsk Vid.-Akad. Skr. No. 8.*

Barth, T. F. W. 1953: The Layered gabbro series at Seiland, Northern Norway. *Norges geol. Unders. 184*, 191–200.

Bottinga, Y. & Weill, D. F. 1970: Densities of liquid silicate systems calculated from partial molar volumes of oxide components *Am. Jour. Sci. 269*, 169–182.

Brown, G. M. 1956: The layered ultrabasic rocks of Rhum, Inner Hebrides *Roy. Soc. London Phil. Trans. Ser. B 240*, 1–53

Brown, G. M. 1967: Mineralogy of basaltic rocks *In* Hess, H. H. & Poldervaart, A. (Eds.), *Basalts*. 1. 103–163. New York: Interscience.

Brown, P. E. 1973: A layered plutonic complex of alkali basalt parentage: The Lilloise intrusion, East Greenland. *Jl. geol. Soc. Lond. 129*, 405–418.

Brown, P. E. & Farmer, D. G. 1972: Size-graded layering in the Imilik gabbro, East Greenland. *Geol. Mag. 108*, 465–575.

Burri, C., Parker, R. L. & Wenk, E. 1967: *Die Optische Orienterung der Plagioclase.* Basel, Birkhauser.

Campbell, I. H. 1978: Some problems with the cumulus theory. *Lithos 11*, 311–323.

Campbell, I. H., Roeder, P. L. & Dixon, J. M. 1978: Plagioclase buoyancy in basaltic liquids as determined with a centrifuge furnace. *Contr. Mineral. and Petrol. 67*, 369–377.
Carmichael, I. S. E., Turner, F. J. & Verhoogen, J. 1974: *Igneous Petrology*. New York, McGraw-Hill Book Co.
Cendrero, A. 1970: The volcano–plutonic complex of La Gomera (Canary Islands). *Bull. Volcan. 34*, 537–561.
Chadwick, G. A. 1972: *Metallography of phase transformations*. London, Butterworths.
Challis, G. A. 1965: The origin of New Zealand ultramafic intrusions. *J. Petrology 6*, 322–364.
Chapman, N. A. 1975: An experimental study of spinel clinopyroxenite xenoliths from the Duncansby Ness vent, Caithness, Scotland. *Contrib. Mineral. Petrol. 51*, 223–230.
Chen, C. F. & Turner, J. S. 1980: Crystallization in a double diffusive system. *J. Geophys. Res. 85*, 2573–2593.
Deer, W. A., Howie, R. A. & Zussman, J. 1962: *Rock Forming Minerals, 5, Non-Silicates*. London, Longmans.
Dickey, J. S. 1970: Partial fusion products in Alpine-type peridotites: Serrania de la Ronda and other examples. *Mineralog. Soc. America Spec. Paper 3*, 33–49.
Donaldson, C. H. 1974: Olivine crystal types in Harrisitic rocks of the Rhum pluton and in Archean spinifex rocks. *Bull. Geol. Soc. Am. 85*, 1721–1726.
Donaldson, C. H. 1975: *A Petrogenetic Study of Harrisite in the Isle of Rhum Pluton, Scotland*. Ph.D. thesis, Univ. of St. Andrews, Scotland.
Donaldson, C. H. 1977: Laboratory duplication of comb layering in the Rhum pluton. *Mineral. Mag. 41*, 323–336.
Drever, H. I. & Johnson, R. 1957: Crystal growth of forsteritic olivine in magmas and melts. *Trans. R. Soc. Edin. 63*, 287–315.
Emslie, R. F. 1965: The Michikamau anorthositic intrusion, Labrador. *Can. J. Earth Sci. 2*, 385–399.
Evans, B. W. & Moore, J. G. 1968: Mineralogy as a function of depth in the prehistoric Makaopuhi tholeiitic lava lake, Hawaii. *Contr. Mineral and Petrol. 17*, 85–115.
Fodor, R. V. & Keil, K. 1975: Contributions to the mineral chemistry of Hawaiian rocks. IV. Pyroxenes in rocks from Haleakala and West Maui volcanoes, Maui, Hawaii. *Contr. Mineral. Petrol. 50*, 173–195.
Fortey, N. J. 1980: Petrofabrics of laminated gabbros from the centre 3 igneous complex, Ardnamurchan, Scotland. *Mineral. Mag. 43*, 989–994.
Fuller, R. E. 1939: Gravitational accumulation of olivine during the advance of basaltic flows. *Jour. Geol. 47*, 303–313.
Gardner, P. M. & Robins, B. 1974: The olivine – plagioclase reaction: Geological evidence from the Seiland Petrographic Province. *Contr. Mineral. and Petrol. 44*, 149–156.
Gastesi, P. 1969: Petrology of the ultramafic and basic rocks of Betancuria massif, Fuerteventura Island (Canarian Archipelago). *Bull. Volcan. 33*, 1008–1038.
Gibb, F. G. 1973: The zoned clinopyroxenes of the Shiant Isles sill, Scotland. *J. Perology 14*, 203–230.
Goode, A. D. T. 1976: Small scale primary cumulus igneous layering in the Kalka layered intrusion, Giles complex, central Australia. *J. Petrology 17*, 379–397.
Grapes, R. H. 1975: Petrology of the Blue Mountain complex, Marlborough, New Zealand. *J. Petrology 16*, 371–428.
Grout, F. F. 1928: Anorthosites and granite as differentiates of a diabase sill on Pigeon Point, Minnesota. *Bull. Geol. Soc. Am. 39*, 555–578.
Harker, A. 1908: The geology of the Small Isles of Inverness-shire (Sheet 60). *Mem. geol. Surv. Scotland*.
Haskin, L., Frey, F., Schmitt, R. & Smith, R. 1966: Meteoric, solar and terrestrial rare earth distributions. *In* Ahrens, L. H. (Ed.): *Physics and Chemistry of the Earth 7*, 167–321. Oxford, Pergamon.
Hess, G. B. 1972: Heat and mass transport during crystallization of the Stillwater igneous complex. *Geol. Soc. America Mem. 132*, 503–520.
Hess, H. H. 1960: Stillwater igneous complex, Montana: a quantitative mineralogical study. *Geol. Soc. America Mem. 80*, 230 pp.
Hoover, J. D. 1978: Petrologic features of the Skaergaard marginal border group. *Carnegie Inst. Wash. Yrbk. 77*, 732–738.

Huppert, H. E. & Sparks, R. S. J. 1980: The fluid dynamics of a basaltic magma chamber replenished by influx of hot, dense ultrabasic magma. *Contr. Mineral. and Petrol. 75*, 279–289.
Irvine, T. N. 1970: Heat transfer during solidification of layered intrusions. I. Sheets and sills. *Can. J. Earth Sci. 7*, 1031–1061.
Irvine, T. N. 1974: Petrology of the Duke Island ultramafic complex, Southeastern Aslaska. *Geol. Soc. America Mem. 138*, 240 pp.
Irvine, T. N. 1978: Infiltration metasomatism, adcumulus growth, and secondary differentiation in the Muskox intrusion. *Carnegie Inst. Wash. Yrbk. 77*, 743–751.
Irvine, T. N. 1979: Rocks whose compositions are determined by crystal accumulation and sorting. *In* Yoder, H. S., Jr. (Ed.): *Evolution of the Igneous Rocks: 50th Anniverssary Perspectives*. Princeton Univ. Press, 245–306.
Irvine, T. N. 1980a: Magmatic density currents and cumulus processes. *Am. Jour. Sci. 280-A*, 1–58.
Irvine, T. N. 1980b: Convection and mixing in layered liquids. *Carnegie Inst. Wash. Yrbk. 79*, 251–256.
Jackson, E. D. 1961: Primary textures and mineral assosiations in the ultramafic zone of the Stillwater complex, Montana. *U.S. Geol. Survey Prof. Paper 358*, 106 pp.
Jackson, E. D. 1967: Ultramafic cumulates in the Stillwater, Great Dyke, and Bushveld intrusions. *In* Wyllie, P. J. (Ed.): *Ultramafic and Related Rocks*, New York, Wiley, 20–38.
Jaeger, J. C. 1957: The temperature in the neighbourhood of a cooling intrusive sheet. *Am. Jour. Sci. 255*, 306–318
Jaeger, J. C. 1964: Thermal effects of intrusions. *Rev. Geophysics 2*, 443–446.
Kingery, W. D. 1959: Sintering in the presence of a liquid phase. *In* Kingery W. D. (Ed.): *Kinetics of High Temperature Processes*. New York, Technical Press and Wiley.
Krauskopf, K. B. 1954: Igneous and metamorphic rocks of the Øksfjord area, Vest-Finnmark. *Norges geol. Unders. 188*, 29–50.
Kuno, H. 1957: Chromian diopside from Sano. Yamanasi Prefecture. *Geol. Soc. Japan Jour. 63*, 523–525.
Kuno, H. 1968: Differentiation of basalt magmas. *In* Hess, H. H. & Poldervaart, A. (Eds.): *Basalts Vol. 2*. New York, Interscience, 623–688.
Kushiro, I. 1969: Stability of omphacite in the presence of excess silica. *Carnegie Inst. Wash. Yrbk. 67*, 98–100.
Leeman, W. P. & Rogers, J. J. W. 1970: Late Cenozoic alkali–olivine basalts of the Basin-Range Province, USA. *Contr. Mineral. and Petrol. 25*, 1–24.
Le Bas, M. J. 1962: The role of aluminium in igneous clinopyroxene with relation to their parentage. *Am. Jour. Sci. 260*, 267–288.
Le Maitre, R. W. 1965: The significance of the gabbroic xenoliths from Gough Island, South Atlantic. *Mineral. Mag. 34*, 303–317.
Lovering, J. F. & White, A. J. R. 1969: Granulitic and eclogitic inclusions from basic pipes at Delegate, Australia. *Contr. Mineral. and Petrol. 21*, 9–52.
Maaløe, S. 1976: The zoned plagioclase of the Skaergaard intrusion, East Greenland. *J. Petrology 17*, 398–419.
Maaløe, S. 1978: The origin of rhythmic layering. *Mineral. Mag. 42*, 337–345.
Manson, V. 1967: Geochemistry of basaltic rocks: Major elements. *In* Hess, H. H. & Poldervaart, A. (Eds.): *Basalts Vol. 1*. New York, Interscience, 215–269.
McBirney, A. R. 1975: Differentiation of the Skaergaard intrusion. *Nature 253*, 691–694.
McBirney, A. R. & Noyes, R. M. 1979: Crystallization and layering of the Skaergaard intrusion. *J. Petrology 20*, 487–554.
Moore, A. C. 1971: The mineralogy of the Gosse Pile ultramafic intrusion, Central Australia. II. Pyroxenes. *Geol. Soc. Australia Jour. 18*, 243–258.
Moore J. G. & Evans, B. W. 1967: The role of olivine in the crystallization of the prehistoric Makaopuhi tholeiitic lava lake, Hawaii. *Contr. Mineral. and Petrol. 15, 202–223.*
Moore, J. G. & Lockwood, J. P. 1973: Origin of comb layering and orbicular structure, Sierra Nevada Batholith, California. *Bull. Geol. Soc. Am. 84*, 1–20.
Morse, S. A. 1968: Layered intrusions and anorthosite genesis. *In* Isachsen, Y. W. (Ed.): *Origin of Anorthosite and Related Rocks. Mem. N.Y. St. Mus. Sci. Serv. 18*, 175–187.
Morse, S. A. 1969: The Kiglapait layered intrusion, Labrador. *Geol. Soc. America Mem. 112*, 146 pp.

Morse, S. A. 1979: Kiglapait geochemistry: I. Systematics, sampling and density. *J. Petrology 20*, 555–590.
Murase, T. & McBirney, A. R. 1973: Properties of some common igneous rocks and their melts at high temperatures. *Bull. Geol. Soc. Am. 84*, 3563–3592.
Olmsted, J. F. 1968: Petrology of the Mineral Lake intrusion, Northwestern Wisconsin. *In* Isachsen, Y. W. (Ed.): Origin of Anorthosite and Related Rocks. *Mem. N.Y. St. Mus. Sci. Serv. 18*, 149–161.
Onuma, K. & Yagi, K. 1971: The join $CaMgSi_2O_6$–$Ca_2MgSi_2O_7$–$CaTiAl_2O_6$ in the system CaO–MgO–Al_2O_3–TiO_2–SiO_2 and its bearing on titanpyroxenes. *Mineral. Mag. 38*, 471–480.
Oosterom, M. G. 1963: The ultramafites and layered gabbro sequences in the granulite facies rocks on Stjernøy, Finnmark, Norway. *Leidse geol. Mededeel. 28*, 179–296.
Pearce, J. A. & Cann, J. R. 1973: Tectonic setting of basic volcanic rocks determined using trace element analyses. *Earth Planet. Sci. Letters 19*, 290–300.
Philpotts, A. R. 1974: The Monteregian Province *In* Sørensen, H. (Ed): *The Alkaline Rocks*. New York, 293–310.
Platen, H. Von 1965: Experimental anatexis and genesis of migmatites. *In* Pitcher, W. S. & Flinn, G. W. (Eds.): *Controls of Metamorphism*. Edinburgh, Oliver & Boyd, 203–218.
Presnall, D. C., Dixon, S. A., Dixon, J. R., O'Donell, T. H., Brenner, N. L., Schrock, R. L. & Dycus, D. W. 1978: Liquidus phase relations on the join diopside–forsterite–anorthite from 1 atm to 20 kbar: Their bearing on the generation and crystallization of basaltic magma. *Contr. Mineral. and Petrol. 66*, 203–220.
Richter, D. H. & Moore, J. G. 1966: Petrology of the Kilauea Iki lava lake, Hawaii. *U.S. Geol. Survey Prof. paper 537-B*.
Roeder, P. L. & Emslie, R. F. 1970: Olivine-liquid equilibrium. *Contr. Mineral and Petrol. 29*, 275–289.
Robins, B. 1972: Syenite–carbonatite relationships in the Seiland gabbro province, Northern Norway. *Norges geol. Unders. 272*, 43–58.
Robins, B. 1973: Crescumulate layering in a gabbroic body on Seiland, Northern Norway. *Geol. Mag. 109*, 533–542.
Robins, B. 1974: Synorogenic alkaline pyroxenite dykes on Seiland, Northern Norway. *Norsk geol. Tidsskr. 54*, 247–268.
Robins, B. 1975: Ultramafic nodules from Seiland, Northern Norway. *Lithos 8*, 15–27.
Robins, B. & Gardner, P. M. 1974: Synorogenic layered basic intrusions in the Seiland Petrographic Province, Finnmark. *Norges geol. Unders. 312*, 91–130.
Robins, B. & Takla, M. A. 1979: Geology and geochemistry of a metamorphosed picrite–ankaramite dyke suite from the Seiland province, Northern Norway. *Norsk geol. Tidsskr. 59*, 67–95.
Robins, B. & Tysseland, M. 1979: Fenitization of some mafic igneous rocks in the Seiland province, Northern Norway. *Norsk geol. Tidsskr. 59*, 1–23.
Shaw, H. R. 1969: Rheology of basalt in the melting range. *J. Petrology 10*, 510–535.
Skinner, B. J. 1966: Thermal expansion. *In* Clark, S. P. (Ed.): *Handbook of Physical Constants. Geol. Soc. America Mem. 97*.
Smith, J. R. 1958: Optical properties of heated plagioclases. *Am. Mineralogist 43*, 1179–1194.
Smith, J. R. 1974: *Feldspar minerals Vol. 1*. Berlin, Springer.
Sturt, B. A., Pringle, I. R. & Ramsay, D. M. 1978: The Finnmarkian phase of the Caledonian orogeny. *Geol. Soc. London Quart. Journ. 135*, 597–610.
Taubeneck, W. H. & Poldervaart, A. 1960: Geology of the Elkhorn Mountains, Northwestern Oregon: Part 2. Willow Lake intrusion. *Geol. Soc. America Bull. 71*, 1295–1322
Thompson, R. N. 1974: Some high-pressure pyroxenes. *Mineral. Mag. 36*, 768–787.
Tuttle, O. F. & Bowen, N. L. 1958: Origin of granite in the light of experimental studies in the system $NaAlSi_3O_8$ – $KAlSi_3O_8$ – SiO_2 – H_2O. *Geol. Soc. America Mem. 74*.
Tyrrell, G. W. 1917: The picrite–teschenite sill of Lugar (Ayrshire). *Geol. Soc. London Quart. Jour. 72*, 84–131.
Voll, G. 1960: New work on petrofabrics. *Liverpool and Manchester Geol. Jour. 2*, 503–567.
Wadsworth, W. J. 1961: The layered ultrabasic rocks of south-west Rhum, Inner Hebrides. *Roy. Soc. London Phil. Trans. Ser. B 224*, 21–64.

Wadsworth, W. J. 1973: Magmatic sediments. *Minerals Sci. Engng. 5*, 25–35.
Wager, L. R. 1963: The mechanism of adcumulus growth in the layered series of the Skaergaard intrusion. *Mineralog. Soc. America Spec. Paper 1*, 1–19.
Wager, L. R. 1968: Rhythmic and cryptic layering in mafic and ultramafic plutons. *In* Hess, H. H. & Poldervaart, A. (Eds.): *Basalts Vol. 2*, New York, Interscience, 573–622.
Wager, L. R., Brown, G. M. & Wadsworth, W. J. 1960: Types of igneous cumulates. *J. Petrology 1*, 73–85.
Wager, L. R. & Brown, G. M. 1968: *Layered Igneous Rocks*. Edinburgh. Oliver & Boyd.
Wager, L. R. & Deer, W. A. 1939: Geological investigations in East Greenland, Part III. The petrology of the Skaergaard intrusion, Kangerdlugssuaq, East Greenland. *Medd. om Grønland 105*, 352 pp.
Warnaars, F. W. 1967: Petrography of a peridotite-, amphibolite- and gabbro-bearing polyorogenic terrain N.W. of Santiago de Compostela (Spain). *Dept. Petr. Min. Cryst., Univ. Leyden, 2nd. series 30*, 1–208.
Wilkinson, J. F. G. 1967: The petrography of basaltic rocks. *In* Hess, H. H. & Poldervaart, A. (Eds): *Basalts Vol. 1*, New York, Interscience, 163–214.
Wilkinson, J. F. G. 1974: The mineralogy and petrography of alkali basaltic rocks. *In* Sørensen, H. (Ed.): *The Alkaline Rocks*. London, Wiley, 67–95.
Williams, H. 1933: Geology of Tahiti, Moorea and Maiao. *B.P. Bishop Mus. Bull. 105*.
White, R. W. 1966: Ultramafic inclusions in basaltic rocks from Hawaii. *Contr. Mineral. and Petrol. 12*, 245–314.
Yagi, K. 1965: Gravitative settling of olivine in pillows of an Icelandic basalt. *Am. Jour. Sci. 263*, 914–916.
Yoder, H. S. 1965: Diopside–anorthite-water at five and ten kilobars and its bearing on explosive volcanism. *Carnegie Inst. Wash. Yrbk. 64*, 82–89.
Yoder, H. S. & Tilley, C. E. 1962: Origin of basaltic magmas: An experimental study of natural and synthetic rock systems. *J. Petrology 3*, 342–532.